Partial dynamical symmetry in the symplectic shell model

Jutta Escher*
TRIUMF, 4004 Wesbrook Mall, Vancouver, British Columbia, Canada V6T 2A3

Amiram Leviatan†
Racah Institute of Physics, The Hebrew University, Jerusalem 91904, Israel
(Received 10 October 2001; published 29 April 2002)

We present an example of a partial dynamical symmetry (PDS) in an interacting fermion system and demonstrate the close relationship of the associated Hamiltonians with a realistic quadrupole-quadrupole interaction, thus shedding light on this important interaction. Specifically, in the framework of the symplectic shell model of nuclei, we prove the existence of a family of fermionic Hamiltonians with partial SU(3) symmetry. We outline the construction process for the PDS eigenstates with good symmetry and give analytic expressions for the energies of these states and $E2$ transition strengths between them. Characteristics of both pure and mixed-symmetry PDS eigenstates are discussed and the resulting spectra and transition strengths are compared to those of real nuclei. The PDS concept is shown to be relevant to the description of prolate, oblate, as well as triaxially deformed nuclei. Similarities and differences between the fermion case and the previously established partial SU(3) symmetry in the interacting boson model are considered.

DOI: 10.1103/PhysRevC.65.054309 PACS number(s): 21.60.Fw, 21.10.−k, 27.20.+n, 27.30.+t

I. INTRODUCTION

Symmetries play an important role in physics. Constants of motion associated with a symmetry govern the integrability of a given classical system, and at the quantum level symmetries provide labels for the classification of states, determine selection rules, and simplify the relevant Hamiltonian matrices. Algebraic, symmetry-based, theories have been firmly established as an elegant and practical approach to a variety of physical systems (see, for example, Refs. [1–12]). These theories offer the greatest simplifications when the interaction under consideration is symmetry preserving in the selected state labeling scheme, that is, when the Hamiltonian either commutes with all the generators of a particular group (exact symmetry) or when it is written in terms of and commutes with the Casimir operators of a chain of nested groups (dynamical symmetry). In both cases basis states belonging to inequivalent irreducible representations of the relevant groups do not mix, the Hamiltonian matrix has block structure, and all properties of the system can be expressed in closed form. An exact or dynamical symmetry not only facilitates the numerical treatment of the Hamiltonian, but also its interpretation and thus provides considerable insight into the physics of a given system.

Naturally, the application of exact or dynamical symmetries to realistic situations has its limitations: Usually the assumed symmetry is only approximately fulfilled, and imposing certain symmetry requirements on the Hamiltonian might result in constraints that are too severe and incompatible with experimentally observed features of the system. The standard approach in such situations is to break the symmetry. In cases where a symmetry-breaking Hamiltonian is involved, it is possible to decompose the offending terms into basic parts (irreducible tensor operators) that exhibit specific transformation properties. Provided the appropriate group coupling coefficients and the matrix elements of some elementary tensor operators are available, matrix elements of operators that connect inequivalent irreducible representations can be determined and the exact eigenvalues and eigenstates can then be obtained (at least in principle). While group theoretical considerations still play an important role in evaluating the coupling coefficients and matrix elements for such a calculation and in truncating model spaces that have become too large for a complete numeric treatment, the basic simplicity of the symmetry-based approach is lost.

Alternatively, one might consider some intermediate structure, which allows for symmetry breaking, but preserves the advantages of a dynamical symmetry for a part of the system. Partial dynamical symmetry (PDS) [13] provides such a structure. It corresponds to a particular symmetry breaking for which the Hamiltonian is not invariant under the symmetry group and hence various irreducible represention (irreps) are mixed in its eigenstates, yet it possesses a subset of ''special'' solvable states that respect the symmetry. The notion of partial dynamical symmetry generalizes the concepts of exact and dynamical symmmetries. In making the transition from an exact to a dynamical symmetry, states that are degenerate in the former scheme are split but not mixed in the latter, and the block structure of the Hamiltonian is retained. Proceeding further to partial symmetry, some blocks or selected states in a block remain pure, while other states mix and lose the symmetry character. Quasiexactly solvable models, as discussed in Ref. [14], exhibit a special form of partial symmetry for which the solvable states span complete representations.

Other generalizations of the idea of dynamical symmetry are possible. Van Isacker [15], for example, suggested to break the dynamical symmetry associated with an intermediate group G_2 in a subchain $G_1 \supset G_2 \supset G_3$ for all states of the system, while preserving the remaining (dynamical) symmetries. The resulting Hamiltonian is, in general, not analyti-

*Electronic address: escher@triumf.ca
†Electronic address: ami@vms.huji.ac.il

cally solvable, but its eigenstates can still be (partly) classified by quantum labels associated with the groups G_1 and G_3. An approximate symmetry scheme called quasidynamical symmetry was discussed by Bahri and Rowe [16]. They considered strong but coherent mixing of the irreducible representations associated with a given dynamical symmetry. Both methods of extending the concept of dynamical symmetry differ from the notion of partial dynamical symmetry introduced above since, unlike in the partial-symmetry case, the eigenvalues of the Hamiltonians cannot be obtained analytically, not even for a part of the system.

The partial-symmetry scheme was introduced in bosonic systems, where it was applied to the spectroscopy of deformed nuclei. In Ref. [17], a Hamiltonian with partial SU(3) symmetry was constructed in the framework of the interacting boson model (IBM) of nuclei [6], and the calculated spectrum and $E2$ rates of ^{168}Er were compared to experimental results. The PDS Hamiltonian was found to reproduce the experimentally observed feature of nondegenerate rotational γ and β bands (K-band splitting) and to possess several bands of solvable states, whereas previous attempts to describe the ^{168}Er data had involved Hamiltonians with SU(3) dynamical symmetry, which can only yield γ and β bands with degenerate angular momentum states, or had achieved agreement with the data by completely breaking the SU(3) symmetry. Employing the same Hamiltonian, Sinai and Leviatan [18,19] investigated the structure of the lowest collective $K=0^+$ excitation in deformed rare-earth nuclei. Implications of the partial dynamical symmetry for the mixing behavior of this collective band were discussed and compared to broken-SU(3) predictions. In another study, Ref. [20], in the context of the IBM-2, the proton-neutron version of the interacting boson model [6,21], Talmi was able to explain simple regularities in spectra of the Majorana operator as an example of partial dynamical symmetry. More recently, the relevance of partial F-spin symmetry was studied in the framework of the IBM-2. It has long been known that F spin, the SU(2) quantum number associated with the two-valued proton-neutron degree of freedom of the IBM-2, cannot be conserved in nuclear spectroscopy. However, Leviatan and Ginocchio [22] demonstrated that empirical energy systematics in the deformed Dy-Os region can be reproduced under the assumption of partial F-spin symmetry. Moreover, the associated partial-symmetry Hamiltonians point to the existence of F-spin multiplets of scissors states, with a moment of inertia equal to that of the ground band. These predictions were tested against recent analyses of $M1$ transition strengths.

The subject of partial symmetries and supersymmetry in nuclear physics was considered by Jolos and von Brentano in the context of the interacting boson-fermion model [23] and the particle-rotor model [24].

Partial symmetries can be associated with continuous as well as discrete groups. The dynamical groups employed in the IBM, e.g., are continuous. In Ref. [25], an example of a partial symmetry that involves point groups was presented in the context of molecular physics. Ping and Chen used a model of N coupled anharmonic oscillators to describe the molecule XY_6. The partial symmetry of the Hamiltonian allowed them to derive analytic expressions for the energies of a set of unique levels and to discuss the structure of the associated eigenstates. Furthermore, the numerical calculations required to obtain the energies of the remaining (nonunique) levels were greatly simplified since the Hamiltonian could be diagonalized in a much smaller space.

Partial symmetries have relevance not only for discrete spectroscopy but also for the study of stochastic properties of dynamical systems. A generic classical or quantum-mechanical Hamiltonian exhibits mixed dynamics: areas of regular motion and chaotic regions coexist in phase space, and even when a system seems to be fully chaotic, regular states may exist. Whelan *et al.* [26] used Hamiltonians with partial dynamical symmetries to investigate quantum-mechanical systems that are partly regular and partly chaotic. In the context of the interacting boson model, it was demonstrated that partial symmetries impose a particular phase-space structure that leads to a suppression of chaos in mixed systems. Canetta and Maino [27] carried out a quantum-statistical analysis of regular and chaotic dynamic behavior in the IBM-2. Varying the Hamiltonian parameters, they observed a nearly regular region in parameter space—far away from dynamical symmetry limits—which they linked to the existence of a partial dynamical symmetry. Since Hamiltonians with partial symmetries are not completely integrable and may exhibit stochastic behavior, they are an ideal tool for studying mixed systems with coexisting regularity and chaos.

Partial symmetries are not confined to bosonic systems. In Ref. [28], an example of a partial symmetry in an interacting fermion system was presented. A family of Hamiltonians with partial SU(3) symmetry was introduced in the framework of the symplectic shell model of nuclei [29]. The Hamiltonians were shown to be closely related to the deformation-inducing quadrupole-quadrupole interaction and to possess both mixed-symmetry and solvable pure-SU(3) rotational bands. For the example of the (prolate) deformed light nucleus ^{20}Ne, it was demonstrated that various features of the quadrupole-quadrupole interaction can be reproduced with a particular parametrization of the PDS Hamiltonians. In that work, the partial dynamical symmetry was identified directly at the fermion level. It is also possible to start with a bosonic PDS Hamiltonian and map the bosonic generators into fermionic generators of the same algebra. This approach was taken by Mamistvalov [30], who studied partial symmetry in a schematic $SU(2)\times SU(2)$-type Lipkin model. Very recently, partially solvable shell-model Hamiltonians with seniority-conserving interactions were investigated by Rowe and Rosensteel [31].

It is the purpose of this work to investigate the fermionic PDS Hamiltonians presented in Ref. [28] in more detail. Specifically, the construction process for the pure eigenstates is outlined and analytic expressions for the energies of pure states and the strengths of $E2$ transitions between these states are given. Properties of the special solvable states are discussed and an application to the oblate deformed light nucleus ^{12}C and the prolate nucleus ^{20}Ne are presented. Moreover, an application to ^{24}Mg demonstrates the rel-

evance of the PDS concept for well-deformed, triaxial nuclei.

In the following section, the symplectic shell model (SSM) is reviewed. In Sec. III, a family of symplectic Hamiltonians with partial SU(3) symmetry is introduced and their relation to the quadrupole-quadrupole interaction is established. Properties of the special eigenstates of the PDS Hamiltonians are discussed in Sec. IV, and applications to realistic nuclear systems are presented in Sec. V. In Sec. VI, the fermionic PDS Hamiltonians are compared to the earlier introduced bosonic PDS Hamiltonians [17–19], and Sec. VII summarizes our work. Appendix A contains further relevant material regarding SU(3) coupling coefficients and reduced matrix elements and Appendix B presents expressions for matrix elements of operators employed in the calculations.

II. THE SYMPLECTIC SHELL MODEL

The SSM is an algebraic, fermionic, shell-model scheme that includes multiple $2\hbar\omega$ one particle–one hole excitations. It includes all essential observables for a description of nuclear monopole and quadrupole collective vibrations as well as for rigid and irrotational flow rotations. Since the model allows for intershell excitations and since its observables are expressible in microscopic shell-model terms, it provides a multishell realization of the nuclear shell model [29].

A. Symplectic generators

The symmetry algebra of the symplectic scheme is spanned by one-body operators that are bilinear products in the (relative) position (x_{si}, $i=1,2,3$, $s=1,\ldots,A-1$) and momentum (p_{si}) observables,

$$Q_{ij}=\sum_s x_{si}x_{sj},$$

$$K_{ij}=\sum_s p_{si}p_{sj},$$

$$L_{ij}=\sum_s (x_{si}p_{sj}-x_{sj}p_{si}),$$

$$S_{ij}=\sum_s (x_{si}p_{sj}+p_{si}x_{sj}), \tag{1}$$

where $A-1$ is the number of Jacobi ''particles'' remaining after removal of the center-of-mass contribution. Together the operators generate the 21-dimensional symplectic algebra sp(6,R), that is, the Lie algebra of linear transformations that preserve a skew-symmetric bilinear form on a six-dimensional real vector space. It is the smallest Lie algebra that contains both the quadrupole moments and the many-nucleon kinetic energy, and it has several physically relevant subalgebras. These include gcm(3) and its subalgebra $[R^5]$so(3), associated with the geometric collective model and its rotational limit, respectively, the algebra gl(3,R) of the general linear motion group, as well as su(3) and its subalgebra so(3), associated with the Elliott model and the rotation group, respectively. The sp(6,R) algebra furthermore includes the canonical subalgebras sp(2,R) and sp(4,R), which have been studied by Arickx *et al.* [32,33], and by Peterson and Hecht [34], respectively, as possible approximations to the full three-dimensional symplectic model.

For many purposes, it is advantageous to express the symplectic generators in terms of harmonic oscillator boson creation and annihilation operators $b^\dagger_{si}=(x_{si}-ip_{si})/\sqrt{2}$ and $b_{si}=(x_{si}+ip_{si})/\sqrt{2}$. The symplectic generators may then be expressed as one-body operators that are quadratic in the oscillator bosons [35]

$$A_{ij}=\frac{1}{2}\sum_s b^\dagger_{si}b^\dagger_{sj},$$

$$B_{ij}=\frac{1}{2}\sum_s b_{si}b_{sj},$$

$$C_{ij}=\frac{1}{2}\sum_s (b^\dagger_{si}b_{sj}+b_{sj}b^\dagger_{si}). \tag{2}$$

Alternatively, one may use the spherical components of the oscillator bosons, $b^{\dagger(10)}_{s,1,\pm1}=\mp(b^\dagger_{s1}\pm ib^\dagger_{s2})/\sqrt{2}$, $b^{\dagger(10)}_{s,1,0}=b^\dagger_{s3}$, and $\tilde{b}^{(01)}_{s,1,\pm1}=\mp(b_{s1}\pm ib_{s2})/\sqrt{2}$, $\tilde{b}^{(01)}_{s,1,0}=b_{s3}$, to write the generators as SU(3) tensor operators [36,37],

$$\hat{H}_0=\sqrt{3}\sum_s \{b^{\dagger(10)}_s\times\tilde{b}^{(01)}_s\}^{(00)}_{00}+\frac{3}{2}(A-1),$$

$$\hat{C}^{(11)}_{lm}=\sqrt{2}\sum_s \{b^{\dagger(10)}_s\times\tilde{b}^{(01)}_s\}^{(11)}_{lm}\quad(l=1,2),$$

$$\hat{A}^{(20)}_{lm}=\frac{1}{\sqrt{2}}\sum_s \{b^{\dagger(10)}_s\times b^{\dagger(10)}_s\}^{(20)}_{lm}\quad(l=0,2),$$

$$\hat{B}^{(02)}_{lm}=\frac{1}{\sqrt{2}}\sum_s \{\tilde{b}^{(01)}_s\times\tilde{b}^{(01)}_s\}^{(02)}_{lm}\quad(l=0,2). \tag{3}$$

The notation $T^{(\lambda,\mu)}_{lm}$ indicates that the operator T possesses good SU(3) [superscript (λ,μ)] and SO(3) (subscript lm) tensorial properties. Since $b^\dagger_s b^\dagger_s$ adds two quanta to particle s, thereby moving it up across two major oscillator shells, $\hat{A}^{(20)}_{lm}$ creates a $2\hbar\omega$ excitation in the system. Analogously, $\hat{B}^{(02)}_{lm}$, which is related to $\hat{A}^{(20)}_{lm}$ by Hermitian conjugation, $\hat{B}^{(02)}_{lm}=(-1)^{l-m}(\hat{A}^{(20)}_{l-m})^\dagger$, annihilates a $2\hbar\omega$ excitation. The $\hat{C}^{(11)}_{lm}$ act only *within* a major harmonic oscillator shell. They generate the group SU(3) of the well-known Elliott model [38],

$$\sqrt{3}\hat{C}^{(11)}_{2m}=Q^E_{2m}\equiv\sqrt{\frac{4\pi}{5}}\sum_s [r^2_s Y_{2m}(\hat{r}_s)+p^2_s Y_{2m}(\hat{p}_s)]$$

$$(m=0,\pm1,\pm2),$$

$$\hat{C}^{(11)}_{1q}=\hat{L}_q\quad(q=0,\pm1), \tag{4}$$

where Q^E_{2m} denotes the symmetrized quadrupole operator of Elliott, which does not couple different major shells, and $\hat{L}_q$ is the orbital angular momentum operator. The harmonic oscillator Hamiltonian $\hat{H}_0=\Sigma_{i=1}^3\hat{C}_{ii}$ is a SU(3) scalar and generates U(1) in U(3)=SU(3)×U(1).

Alternatively, one can realize the symplectic generators in terms of fermionic creation and annihilation operators [36],

$$\hat{C}^{(11)}_{lm}=\sum_\eta \sqrt{\frac{1}{6}\eta(\eta+1)(\eta+2)(\eta+3)}\{a^\dagger_\eta\times\tilde{a}_\eta\}^{(11)S=0}_{lm\Sigma=0} + \hat{\mathcal{O}}^{cm}_C(A),$$

$$\hat{A}^{(20)}_{lm}=\sum_\eta \sqrt{\frac{1}{12}(\eta+1)(\eta+2)(\eta+3)(\eta+4)} \times\{a^\dagger_{\eta+2}\times\tilde{a}_\eta\}^{(20)S=0}_{lm\Sigma=0}+\hat{\mathcal{O}}^{cm}_A(A),$$

$$\hat{B}^{(02)}_{lm}=\sum_\eta \sqrt{\frac{1}{12}(\eta+1)(\eta+2)(\eta+3)(\eta+4)} \times\{a^\dagger_\eta\times\tilde{a}_{\eta+2}\}^{(02)S=0}_{lm\Sigma=0}+\hat{\mathcal{O}}^{cm}_B(A), \quad (5)$$

where $a^\dagger_{\eta lm1/2\sigma}$ [$\tilde{a}_{\eta lm1/2\sigma}=(-1)^{\eta+l+m+1/2+\sigma}a_{\eta l-m1/2-\sigma}$] is a single-particle creation (annihilation) operator, which produces (destroys) a fermion with angular momentum l, projection m, and spin 1/2, projection σ in the ηth major oscillator shell. The sums run over all shells, and the coupling to total spin $S=0$ with projection $\Sigma=0$ reflects the fact that the generators act on spatial degrees of freedom only. The operators $\hat{\mathcal{O}}^{cm}(A)$ remove the spurios center-of-mass content from the generators. Details regarding the fermionic realization of Sp(6,R) can be found in Ref. [36].

B. Symplectic basis states

A basis for the symplectic model is generated by applying symmetrically coupled products of the $2\hbar\omega$ raising operator $\hat{A}^{(20)}$ with itself to the usual $0\hbar\omega$ many-particle shell-model states. Each $0\hbar\omega$ starting configuration is characterized by the distribution of oscillator quanta into the three cartesian directions $\{\sigma_1,\sigma_2,\sigma_3\}$, where $\sigma_1\geqslant\sigma_2\geqslant\sigma_3$. Here σ_i denotes the eigenvalue of the U(3) weight operator $C_{ii}=\Sigma_s(b^\dagger_{si}b_{si}+1/2)$, which essentially counts the number of oscillator bosons in the ith direction of the system. Since $s=1,2,\ldots,A-1$, it follows that the σ_i are half-integer numbers for even-A and integers for odd-A nuclei. Equivalently, one may employ quantum numbers $N_\sigma(\lambda_\sigma,\mu_\sigma)$, where $\lambda_\sigma=\sigma_1-\sigma_2$, $\mu_\sigma=\sigma_2-\sigma_3$ are the Elliott SU(3) labels, and $N_\sigma=\sigma_1+\sigma_2+\sigma_3$ is the eigenvalue of the harmonic oscillator Hamiltonian $\hat{H}_0=\hat{C}_{11}+\hat{C}_{22}+\hat{C}_{33}$, which takes the minimum value consistent with the Pauli exclusion principle. Each such set of U(3) quantum numbers uniquely determines an irrep of the symplectic algebra, since it characterizes a sp(6,R) lowest weight state. Note that a lowest weight vector of sp(6,R) is also a lowest weight state of its u(3) subalgebra.

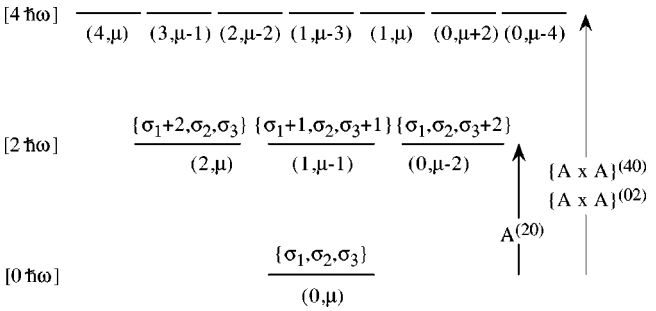

FIG. 1. Basis construction in the symplectic model. SU(3)-coupled products of the raising operator $\hat{A}^{(20)}$ with itself act on an Elliott starting state with $(\lambda_\sigma,\mu_\sigma)=(0,\mu)$ ($\{\sigma_1,\sigma_2=\sigma_1,\sigma_3\}$) to generate symplectic $2\hbar\omega$, $4\hbar\omega$, ... excitations. Also shown are the SU(3) labels (λ,μ) and quanta distributions $\{\omega_1,\omega_2,\omega_3\}$ for some excited states.

Any component of the symplectic lowering operator $B^{(02)}$ (and of $\hat{C}_{ij}$ with $i<j$) annihilates such a lowest weight state.

In contrast, application of the symplectic generator $\hat{A}^{(20)}$ to this lowest weight vector allows one to successively build a basis for the sp(6,R) irrep under consideration: The product of $N/2$, $N=0,2,4,\ldots$, raising operators $\hat{A}^{(20)}$ is multiplicity-free and generates $N\hbar\omega$ excitations for each starting configuration $N_\sigma(\lambda_\sigma,\mu_\sigma)$. Each such product operator $\mathcal{P}^{N(\lambda_n,\mu_n)}$ can be labeled according to its U(3) content, $\{n_1,n_2,n_3\}$ or $N(\lambda_n,\mu_n)$, where (λ_n,μ_n) ranges over the set

$$\Omega=\{(n_1-n_2,n_2-n_3)|n_1\geqslant n_2\geqslant n_3\geqslant 0; \quad N=n_1+n_2+n_3; n_1,n_2,n_3 \text{ even integers}\}. \quad (6)$$

The raising polynomial $\mathcal{P}^{N(\lambda_n,\mu_n)}$ is then coupled with $|N_\sigma(\lambda_\sigma,\mu_\sigma)\rangle$ to good SU(3) symmetry $\rho(\lambda_\omega,\mu_\omega)$, with ρ denoting the multiplicity in the coupling $(\lambda_n,\mu_n)\otimes(\lambda_\sigma,\mu_\sigma)$. The quanta distribution in the associated lowest weight state is given by $\{\omega_1,\omega_2,\omega_3\}$, with $N_\omega\equiv N_\sigma+N=\omega_1+\omega_2+\omega_3$, $\omega_1\geqslant\omega_2\geqslant\omega_3$ and $\lambda_\omega=\omega_1-\omega_2$, $\mu_\omega=\omega_2-\omega_3$. The states of the Sp(6,R) $\supset$ SU(3) basis are thus labeled by three types of U(3) quantum numbers: $\Gamma_\sigma\equiv\{\sigma_1,\sigma_2,\sigma_3\}=N_\sigma(\lambda_\sigma,\mu_\sigma)$, the symplectic bandhead or Sp(6,R) lowest weight U(3) symmetry, which specifies the sp(6,R) irreducible representation; $\Gamma_n\equiv\{n_1,n_2,n_3\}=N(\lambda_n\mu_n)$, the U(3) symmetry of the raising polynomial; and $\Gamma_\omega\equiv\{\omega_1,\omega_2,\omega_3\}=N_\omega(\lambda_\omega,\mu_\omega)$, the U(3) symmetry of the coupled product. A given symplectic representation space $N_\sigma(\lambda_\sigma,\mu_\sigma)$ is infinite dimensional, since $N/2$, the number of oscillator excitations, can take any non-negative integer value. In practical applications, one must, therefore, either truncate the symplectic Hilbert space, or restrict oneself to interactions and observables for which the matrix elements depend solely on the symplectic irrep and can be calculated analytically. The basis state construction is schematically illustrated in Fig. 1 for a typical Elliott starting state with $(\lambda_\sigma,\mu_\sigma)=(0,\mu)$. A similar figure for $(\lambda_\sigma,\mu_\sigma)=(\lambda,0)$ is given in Ref. [28].

To complete the basis state labeling, additional quantum numbers α are required. This can be accomplished by reducing Sp(6,R) $\supset$SU(3) states with respect to the subgroup U(1)$\times$SU(2) of SU(3) and assigning labels $\alpha=\varepsilon\Lambda M_\Lambda$ [39]. This SU(2) subgroup, however, is not the physical orbital angular momentum subgroup SO(3) of SU(3). States with good angular momentum values can be obtained from the SU(3)$\supset$U(1)$\times$SU(2) (canonical) basis by projection [38,40]. The associated quantum numbers are $\alpha=\kappa LM$, where κ is a multiplicity index, which enumerates multiple occurrences of a particular L value in the SU(3) irrep (λ,μ) from 1 to $\kappa_L^{max}(\lambda,\mu)$,

$$\kappa_L^{max}(\lambda,\mu)=[(\lambda+\mu+2-L)/2]-[(\lambda+1-L)/2] -[(\mu+1-L)/2], \tag{7}$$

where $[\cdots]$ is the greatest non-negative integer function [41]. The $\kappa_L^{max}(\lambda,\mu)$ occurrences of L can be distinguished in a variety of ways. The physically most significant scheme is that of Elliott [38], in which case the projection of L along the body-fixed three-axis, denoted K, is used to sort the L values into the familiar K bands of the rotational model. Unfortunately, states defined in this manner are not orthonormal with respect to the multiplicity quantum number K [42]. To avoid the resulting complications, such as working with non-Hermitian matrices, the Elliott basis is usually orthonormalized using a Gram-Schmidt process. Vergados [43], for example, gives a prescription to construct orthogonal basis states in a systematic manner for all (λ,μ), such that the physical interpretation of K as a band label can be approximately maintained [44]. In the present work, we employ the orthonormal basis of Vergados. For simplicity, however, we use the running index $\kappa=1,2,\ldots,\kappa_L^{max}$ to distinguish multiple occurrences of L in a given SU(3) irrep (λ,μ) and list the corresponding Vergados labels where appropriate. The dynamical symmetry chain and the associated quantum labels of the above scheme are given by [29]:

$$\begin{array}{ccccccccc} \mathrm{Sp}(6,R) & \supset & \mathrm{U}(3) & \supset & \mathrm{SO}(3) & \supset & \mathrm{SO}(2) \\ N_\sigma(\lambda_\sigma,\mu_\sigma) & & N(\lambda_n,\mu_n)\rho & & N_\omega(\lambda_\omega,\mu_\omega) & \kappa & L & & M \end{array} \tag{8}$$

When applying the formalism to realistic nuclei, we assign rotational band labels according to the calculated $B(E2)$ rates.

The quadratic Casimir operators of SU(3) and Sp(6,R),

$$\hat{C}_{\mathrm{SU3}}=\frac{1}{2}[C_2^{(11)}\cdot C_2^{(11)}+C_1^{(11)}\cdot C_1^{(11)}], \tag{9}$$

$$\hat{C}_{\mathrm{Sp(6)}}=-2\hat{A}_0^{(20)}\cdot\hat{B}_0^{(02)}-2\hat{A}_2^{(20)}\cdot\hat{B}_2^{(02)}+\hat{C}_{\mathrm{SU(3)}} +\frac{1}{3}\hat{H}_0{}^2-4\hat{H}_0, \tag{10}$$

have the following eigenvalues in the dynamical symmetry basis:

$$\langle\hat{C}_{\mathrm{SU(3)}}\rangle[(\lambda,\mu)]=2(\lambda^2+\mu^2+\lambda\mu+3\lambda+3\mu)/3, \tag{11}$$

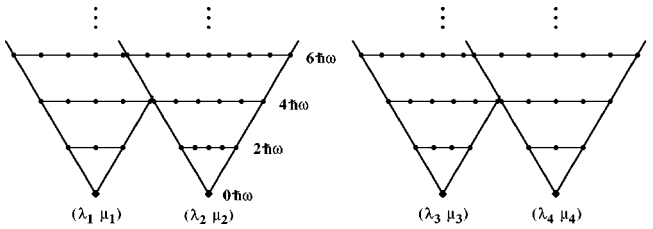

FIG. 2. Symplectic shell-model space. The schematic plot illustrates a model space with multiple symplectic representations. Each ''cone'' corresponds to a sp(6,R) irrep and is uniquely characterized by U(3) quantum numbers $N_\sigma(\lambda_\sigma,\mu_\sigma)$, where $(\lambda_\sigma,\mu_\sigma)$ denotes the Elliott SU(3) quantum labels for the associated $0\hbar\omega$ shell-model configuration. For a given starting representation $(\lambda_\sigma,\mu_\sigma)$ ($\sigma=1,2,3,4$ here), one obtains multiple SU(3) configurations, $(\lambda_\omega,\mu_\omega)$, at each $N\hbar\omega$ level of excitation ($N>0$), indicated here by small filled circles.

$$\langle\hat{C}_{\mathrm{Sp(6)}}\rangle[N_\sigma(\lambda_\sigma,\mu_\sigma)] =2(\lambda_\sigma^2+\mu_\sigma^2+\lambda_\sigma\mu_\sigma+3\lambda_\sigma+3\mu_\sigma)/3+N_\sigma^2/3-4N_\sigma. \tag{12}$$

The collection of all $0\hbar\omega$ configurations provides a complete Hilbert space for the Elliott SU(3) submodel of the SSM and is referred to as the $0\hbar\omega$ horizontal shell-model space. The set of states built on a given U(3) irrep $N_\sigma(\lambda_\sigma\mu_\sigma)$ is called the vertical extension of that irrep. Each vertical extension can be partitioned into horizontal slices with the states within the $(N/2)$th slice representable as a homogeneous polynomial of degree $N/2$ in the $\hat{A}^{(20)}$ tensors acting on the parent $0\hbar\omega$ configuration (see also Fig. 2). Interactions can thus be classified according to their effect on this structure; pairing, for example, causes horizontal mixing, both within each ''cone'' (symplectic irrep) and between different cones, while the quadrupole-quadrupole interaction induces horizontal and vertical mixing, but does not connect different cones.

C. Symplectic Hamiltonians

A primary goal of the symplectic shell model is to achieve a microscopic description of deformed nuclei. These nuclei exhibit collective behavior, that is, modes of excitation in which an appreciable fraction of the nucleons in the system participate in a coherent manner, as, for example, is the case for rotations. An appropriate Hamiltonian for describing rotational phenomena within the symplectic model consists of the harmonic oscillator, which provides the background shell structure, the quadrupole-quadrupole interaction $Q_2\cdot Q_2$, and a residual interaction that should include, for example, single-particle spin orbit and orbit-orbit terms, as well as pairing and other interactions. However, most applications of the theory are much less ambitious than this, restricting the interaction to terms that can be expressed solely in terms of generators of the symplectic algebra [29,45–47]. Interactions of the latter form do not mix different symplectic irreps and, therefore, the Hamiltonian matrix for such interactions becomes block diagonal. Indeed, in most practical applications

the Hilbert space of the system is truncated to one single symplectic representation. This is accomplished by selecting the vertical slice (symplectic irrep) constructed from the leading starting irrep of the $0\hbar\omega$ space. The leading irrep is defined to be the U(3) representation, $N_\sigma(\lambda_\sigma,\mu_\sigma)$, from the lowest layer with the most symmetric spatial permutation symmetry consistent with the Pauli principle, and the maximal possible SU(3) Casimir operator value, $\langle\hat{C}_{\mathrm{SU(3)}}\rangle[(\lambda_\sigma,\mu_\sigma)]$. For ^{12}C, for instance, the leading irrep is given by N_σ $(\lambda_\sigma,\mu_\sigma)=24.5$ (0,4), which corresponds to the symplectic weights $\sigma_1=\sigma_2=9.5$, $\sigma_3=5.5$; for ^{20}Ne, one finds $N_\sigma(\lambda_\sigma,\mu_\sigma)=48.5$ (8,0), since $\sigma_1=21.5$, $\sigma_2=\sigma_3=13.5$ [29]; and ^{24}Mg has $N_\sigma(\lambda_\sigma,\mu_\sigma)=62.5$ (8,4), that is, $\sigma_1=27.5$ $\sigma_2=19.5$, $\sigma_3=15.5$ [46]. The single symplectic irrep approximation is a sensible choice for nuclear systems that have a dominant quadrupole-quadrupole force, since this interaction does not mix symplectic representations and favors states with large $\langle\hat{C}_{\mathrm{SU(3)}}\rangle[(\lambda_\sigma,\mu_\sigma)]$ values.

A typical Hamiltonian for a calculation in a space truncated in the manner described above, is given by a harmonic oscillator term H_0 plus a collective potential, and a residual interaction:

$$H=H_0+V_{coll}+V_{res}. \tag{13}$$

We choose the collective potential to be a simple quadratic, rotationally invariant, function of the microscopic quadrupole moment [48], $Q_{2m}=\sqrt{(16\pi)/5}\Sigma_s r_s^2 Y_{2m}(\hat{r}_s)$, namely,

$$V_{coll}=-\chi Q_2\cdot Q_2. \tag{14}$$

The quadrupole-quadrupole interaction is a standard ingredient in models that aim at reproducing rotational spectra and nuclear deformations. It emerges (apart from a constant) as a leading contribution in the multipole expansion of a general two-body force. It mixes states from different oscillator shells, since the quadrupole operator has nonvanishing matrix elements between shells differing by zero or two oscillator quanta. A major strength of the symplectic model is its ability to fully accommodate the action of the quadrupole operator, which can be written in terms of symplectic generators,

$$Q_{2m}=\sqrt{3}(\hat{C}^{(11)}_{2m}+\hat{A}^{(20)}_{2m}+\hat{B}^{(02)}_{2m}). \tag{15}$$

As a result, the model is able to reproduce intraband and interband $E2$ transition strengths between low lying, as well as giant resonance, states without introducing proton and neutron effective charges.

The effective residual interaction V_{res} is included to replace noncollective components of a more realistic Hamiltonian and the neglected effects of couplings to other sp(6,R) representations. As in previous works, we choose V_{res} to be a rotationally invariant function of the SU(3) generators. For prolate and oblate nuclei we use,

$$V_{res}=d_2\hat{L}^2+d_4\hat{L}^4, \tag{16}$$

where $\hat{L}$ denotes the angular momentum operator, Eq. (4). This allows us to reproduce the energy splittings between states of a rotational band. For triaxial nuclei, such as ^{24}Mg, it becomes necessary to include further terms, in order to reproduce the experimentally observed "K-band splitting," the energy differences found between states with the same angular momentum but different K-band assignments. This can be achieved by including "SU(3)$\supset$SO(3) integrity basis" operators $\hat{X}_3\equiv(\hat{L}\times Q^E)_{(1)}\cdot\hat{L}$ and $\hat{X}_4\equiv(\hat{L}\times Q^E)_{(1)}\cdot(\hat{L}\times Q^E)_{(1)}$ in the residual interaction [49]:

$$V'_{res}=c_3\hat{X}_3+c_4\hat{X}_4+d_2\hat{L}^2+d_4\hat{L}^4. \tag{17}$$

The evaluation procedure for the matrix elements of the symplectic generators $A^{(20)}$, $B^{(02)}$, and $C^{(11)}$, and of the integrity basis operators $\hat{X}_3$ and $\hat{X}_4$ is discussed in Appendix B.

III. PDS HAMILTONIANS AND THE QUADRUPOLE-QUADRUPOLE INTERACTION

In this section we introduce a family of fermionic Hamiltonians with partial dynamical symmetry. Motivated by the fact that a realistic quadrupole-quadrupole interaction breaks SU(3) symmetry within a given major oscillator shell, we define a family of Hamiltonians $H(\beta_0,\beta_2)$, which allows us to study the features of the symmetry-breaking terms in some detail. The Hamiltonians do not couple different oscillator shells and, for a particular choice of the parameters β_0 and β_2, reduce to a form that is closely related to the quadrupole-quadrupole interaction restricted to a shell. We prove that this family of Hamiltonians exhibits partial SU(3) symmetry and give rules for determining the "special" irreps and the associated pure eigenstates.

In the symplectic shell model, the quadrupole-quadrupole interaction can be expressed in terms of symplectic generators [50],

$$Q_2\cdot Q_2=3(\hat{C}_2+\hat{A}_2+\hat{B}_2)\cdot(\hat{C}_2+\hat{A}_2+\hat{B}_2). \tag{18}$$

Employing the commutation relations $\hat{B}_2\cdot\hat{A}_2-\hat{A}_2\cdot\hat{B}_2=\frac{10}{3}\hat{H}_0$ and $\hat{B}_2\cdot\hat{C}_2-\hat{C}_2\cdot\hat{B}_2=20\hat{B}_0/\sqrt{6}$, given in Ref. [50], this can be rewritten as

$$\begin{aligned}Q_2\cdot Q_2=&\,3\hat{C}_2\cdot\hat{C}_2+6\hat{A}_2\cdot\hat{B}_2+10\hat{H}_0\\&+[(6\hat{C}_2\cdot\hat{B}_2+10\sqrt{6}\hat{B}_0+3\hat{B}_2\cdot\hat{B}_2)+\mathrm{H.c.}],\end{aligned} \tag{19}$$

where $3\hat{C}_2\cdot\hat{C}_2=Q_2^E\cdot Q_2^E$ and H.c. denotes the Hermitian conjugate of the expression in parentheses. The first three terms in the expansion, Eq. (19), act solely within a major harmonic oscillator shell, while the second line connects states differing in energy by $\pm2\hbar\omega$ and $\pm4\hbar\omega$. It is primarily the presence of the multi-$\hbar\omega$ correlations that differentiates the SSM from the Elliott SU(3) model. The symplectic model allows for coherent multishell admixtures in its wave functions and thus achieves the experimentally observed

nuclear deformation and absolute $B(E2)$ rates. In contrast, the Elliott model requires effective charges, since it employs the algebraic (or Elliott) quadrupole-quadrupole interaction,

$$Q_2^E \cdot Q_2^E = 6\hat{C}_{\mathrm{SU(3)}} - 3\hat{L}^2, \tag{20}$$

which does not connect different oscillator shells.

Although matrix elements of Q_2 and Q_2^E are identical within a harmonic oscillator shell, the corresponding quadrupole-quadrupole interactions exhibit differences here as well: The $\hat{C}_2 \cdot \hat{C}_2$ and $\hat{H}_0$ terms in the expansion, Eq. (19), are diagonal in the dynamical symmetry basis, Eq. (8), whereas $A_2 \cdot B_2$ contains contributions that mix different SU(3) irreps. This follows from the relations

$$\hat{A}_0 \cdot \hat{B}_0 \equiv \hat{A}_0^{(20)} \cdot \hat{B}_0^{(02)} = \frac{1}{\sqrt{6}} \{\hat{A} \times \hat{B}\}_0^{(00)} - \sqrt{\frac{5}{6}} \{\hat{A} \times \hat{B}\}_0^{(22)},$$

$$\hat{A}_2 \cdot \hat{B}_2 \equiv \hat{A}_2^{(20)} \cdot \hat{B}_2^{(02)} = \frac{5}{\sqrt{6}} \{\hat{A} \times \hat{B}\}_0^{(00)} + \sqrt{\frac{5}{6}} \{\hat{A} \times \hat{B}\}_0^{(22)}, \tag{21}$$

where

$$\{\hat{A} \times \hat{B}\}_0^{(00)} = \frac{1}{2\sqrt{6}} \left(\hat{C}_{\mathrm{SU(3)}} + \frac{1}{3}\hat{H}_0^2 - 4\hat{H}_0 - \hat{C}_{\mathrm{Sp(6)}} \right). \tag{22}$$

The term $\{\hat{A} \times \hat{B}\}_0^{(00)}$ is a SU(3) scalar, but $\{\hat{A} \times \hat{B}\}_0^{(22)}$ breaks SU(3) symmetry. Within a major oscillator shell, it is mainly this symmetry-breaking term that distinguishes the action of $Q_2 \cdot Q_2$ from the effect of the Elliott interaction $Q_2^E \cdot Q_2^E$, which respects the symmetry.

To explore this latter aspect in more detail, we rewrite the collective quadrupole-quadrupole interaction as follows:

$$Q_2 \cdot Q_2 = 9\hat{C}_{\mathrm{SU(3)}} - 3\hat{C}_{\mathrm{Sp(6)}} + \hat{H}_0^2 - 2\hat{H}_0 - 3\hat{L}^2 - 6\hat{A}_0\hat{B}_0 + \{\text{terms coupling different h.o. shells}\}. \tag{23}$$

The quadratic Casimir invariants of SU(3), $\hat{C}_{\mathrm{SU(3)}}$, and of Sp(6,R), $\hat{C}_{\mathrm{Sp(6)}}$, and their eigenvalues, are given in Eqs. (9)–(12). In order to focus on the action of $Q_2 \cdot Q_2$ within a harmonic oscillator shell, we introduce the following family of rotationally invariant Hamiltonians:

$$\begin{aligned} H(\beta_0, \beta_2) &= \beta_0 \hat{A}_0 \cdot \hat{B}_0 + \beta_2 \hat{A}_2 \cdot \hat{B}_2 \\ &= \frac{\beta_2}{18}(9\hat{C}_{\mathrm{SU(3)}} - 9\hat{C}_{\mathrm{Sp(6)}} + 3\hat{H}_0^2 - 36\hat{H}_0) \\ &\quad + (\beta_0 - \beta_2)\hat{A}_0 \cdot \hat{B}_0. \end{aligned} \tag{24}$$

For $\beta_0 = \beta_2$, one recovers a Sp(6,R)$\supset$SU(3) dynamical symmetry Hamiltonian: $H(\beta_0, \beta_2 = \beta_0)$ contains only SU(3) scalars, that is, it does not mix different SU(3) irreps. Furthermore, all eigenstates at a given $N\hbar\omega$ excitation that belong to the same symplectic and SU(3) irreps are degenerate. Additional SO(3) rotational terms, such as $\hat{L}^2$ and $\hat{L}^4$ split the degeneracies, but do not change the wave functions. For the special choice $\beta_0 = 12$, $\beta_2 = 18$, one finds that $H(\beta_0 = 12, \beta_2 = 18)$ is closely related to the quadrupole-quadrupole interaction,

$$Q_2 \cdot Q_2 = H(\beta_0 = 12, \beta_2 = 18) + \text{const} - 3\hat{L}^2 + \{\text{terms coupling different h.o. shells}\}, \tag{25}$$

where the value of const$= 6\hat{C}_{\mathrm{Sp(6)}} - 2\hat{H}_0^2 + 34\hat{H}_0$ is fixed for a given symplectic irrep $N_\sigma(\lambda_\sigma, \mu_\sigma)$ and $N\hbar\omega$ excitation. Although $H(\beta_0, \beta_2)$ does not couple different harmonic oscillator shells, it contains the SU(3)-symmetry-breaking term $\{\hat{A} \times \hat{B}\}_0^{(22)}$ and is, therefore, expected to exhibit in-shell behavior similar to that of $Q_2 \cdot Q_2$.

From Eq. (21) it follows that $H(\beta_0, \beta_2)$ is generally not SU(3) invariant. We will now show that $H(\beta_0, \beta_2)$ exhibits partial SU(3) symmetry. Specifically, we claim that among the eigenstates of $H(\beta_0, \beta_2)$, there exists a subset of solvable pure-SU(3) states, the SU(3)$\supset$SO(3) classification of which depends on both the Elliott labels $(\lambda_\sigma, \mu_\sigma)$ of the starting state and the symplectic excitation N. In general, we find that all L states in the starting configuration ($N = 0$) are solvable with good SU(3) symmetry $(\lambda_\sigma, \mu_\sigma)$. For excited configurations, with $N > 0$ (N even), we distinguish two possible cases:

(a) $\lambda_\sigma > \mu_\sigma$: the pure states belong to $(\lambda, \mu) = (\lambda_\sigma - N, \mu_\sigma + N)$ at the $N\hbar\omega$ level and have $L = \mu_\sigma + N, \mu_\sigma + N + 1, \ldots, \lambda_\sigma - N + 1$ with $N = 2,4, \ldots$ subject to $2N \leqslant (\lambda_\sigma - \mu_\sigma + 1)$.

(b) $\lambda_\sigma \leqslant \mu_\sigma$: the special states belong to $(\lambda, \mu) = (\lambda_\sigma + N, \mu_\sigma)$ at the $N\hbar\omega$ level and have $L = \lambda_\sigma + N, \lambda_\sigma + N + 1, \ldots, \lambda_\sigma + N + \mu_\sigma$ with $N = 2,4, \ldots$.

To prove the claim, it is sufficient to show that $\hat{B}_0$ annihilates the states in question [since $H(\beta_0 = \beta_2)$ is diagonal in the dynamical symmetry basis]. For $N = 0$ this follows immediately from the fact that the $0\hbar\omega$ starting configuration is a Sp(6,R) lowest weight which, by definition, is annihilated by the lowering operators of the Sp(6,R) algebra. The latter include the components of the generator $\hat{B}^{(02)}$.

For $N > 0$, we have to study the action of the symplectic generator $\hat{B}_0$ in more detail. The operator $\hat{B}_0$ has the form $\hat{B}_0 = \Sigma_s (b_{s1}b_{s1} + b_{s2}b_{s2} + b_{s3}b_{s3})/\sqrt{6}$, i.e., it is a rotational invariant and can remove two oscillator quanta from any one of the three cartesian directions. A state of angular momentum L in a SU(3) irrep can be obtained by angular momentum projection from the lowest weight vector associated with the irrep. Since $\hat{B}_0$ is rotationally invariant, it commutes with this projection operator and, therefore, it suffices to consider the effect of acting with $\hat{B}_0$ on lowest weight vectors. Let $\{\sigma_1, \sigma_2, \sigma_3\}$ be the quanta distribution for a $0\hbar\omega$ lowest weight state with $\lambda_\sigma > \mu_\sigma$. An excited state at the $N\hbar\omega$ level belongs to a SU(3) irrep that is completely characterized by its lowest weight vector. This lowest weight vector contains $N_\omega \equiv \omega_1 + \omega_2 + \omega_3 = \sigma_1 + \sigma_2 + \sigma_3 + N$ oscillator quanta, which are distributed into the three cartesian directions ($i = 1,2,3$) such that $\omega_i \geqslant \sigma_i$. In particular, the lowest weight

vector of the SU(3) irrep $(\lambda,\mu)=(\lambda_\sigma-N,\mu_\sigma+N)$ at $N\hbar\omega$ has the quanta distribution $\{\sigma_1,\sigma_2+N,\sigma_3\}$. Acting with $\hat{B}_0$ on a $N\hbar\omega$ state with quantum labels $(\lambda,\mu)=(\lambda_\sigma-N,\mu_\sigma+N)$ and L results in a $(N-2)\hbar\omega$ state with SU(3) character $(\lambda',\mu')=(\lambda_\sigma-N+2,\mu_\sigma+N-2)$ and angular momentum $L'=L$. The lowest weight vector of the irrep (λ',μ') has the quanta distribution $\{\sigma_1,\sigma_2+N-2,\sigma_3\}$. Note that the symplectic generator $\hat{B}_0$ cannot connect $(\lambda,\mu)=(\lambda_\sigma-N,\mu_\sigma+N)$ at $N\hbar\omega$ with any other irrep (λ'',μ'') at the $(N-2)\hbar\omega$ level, since the lowest weight vector associated with $(\lambda'',\mu'')\neq(\lambda',\mu')$ has fewer oscillator quanta in either the one- or the three-direction than the starting $(0\hbar\omega)$ configuration, i.e., such (λ'',μ'') would belong to a different symplectic representation. Comparing the number of occurrences of a given angular momentum value L in (λ,μ) at $N\hbar\omega$ and (λ',μ') at $(N-2)\hbar\omega$, one finds the following: As long as $\lambda_\sigma-N+1\geqslant\mu_\sigma+N$ holds, the difference $\Delta_L(N)\equiv\kappa_L^{max}(\lambda,\mu)-\kappa_L^{max}(\lambda',\mu')$ is 1 for $L=\mu_\sigma+N,\mu_\sigma+N+1,\ldots,\lambda_\sigma-N+1$, and zero otherwise [with κ_L^{max} as defined in Eq. (7)]. Therefore, when $\Delta_L(N)=1$, a linear combination $|\phi_L(N)\rangle=\Sigma_\kappa c_\kappa|N\hbar\omega(\lambda_\sigma-N,\mu_\sigma+N)\kappa LM\rangle$ exists such that $\hat{B}_0|\phi_L(N)\rangle=0$, and thus our claim for family (a) holds.

The proof for family (b) can be carried out analogously. Here the special irrep $(\lambda,\mu)=(\lambda_\sigma+N,\mu_\sigma)$ is obtained by adding N quanta to the one-direction of the starting configuration. In this case there is no restriction on N, hence family (b) is infinite. Note that adding quanta to the three-direction does *not* yield another family of pure states, since the multiplicity for a given L value in the associated "special" irreps, $(\lambda,\mu)=(\lambda_\sigma,\mu_\sigma-N)$, decreases as N increases, i.e. $\Delta_L(N)\leqslant 0$ for all L and N.

The SU(3) irreps of family (b), $(\lambda,\mu)=(\lambda_\sigma+N,\mu_\sigma)$ at the $N\hbar\omega$ level, span a one-dimensional subspace of the full, three-dimensional, Sp(6,R) model space. This set of irreps can be generated by a sp(2,R) subalgebra of sp(6,R) with generators A_{11}, B_{11}, C_{11}, as was demonstrated by Arickx [32]. Similarly, the SU(3) irreps of family (a), $(\lambda,\mu)=(\lambda_\sigma-N,\mu_\sigma+N)$ at the $N\hbar\omega$ level can be generated by a sp(2,R) algebra with generators A_{22}, B_{22}, C_{22}. However, it needs to be emphasized that the solvable states of the present PDS example span, in general, only *part* of the above SU(3) irreps.

IV. SOLVABLE STATES AND THEIR PROPERTIES

All $0\hbar\omega$ states are eigenstates of $H(\beta_0,\beta_2)$. They are unmixed and span the entire $(\lambda_\sigma,\mu_\sigma)$ irrep. In contrast, for the excited levels $(N>0)$, the pure states span only part of the corresponding SU(3) irrep. There are other states at each excited level that do not preserve the SU(3) symmetry and therefore contain a mixture of SU(3) irreps.

To construct the pure states for $N>0$, we proceed as follows: Let (λ,μ) at $N\hbar\omega$ be the irrep that contains a pure state with angular momentum L and projection M, $|\phi_{LM}(N)\rangle$. This state can be written as

$$|\phi_{LM}(N)\rangle=\sum_{\kappa=1}^{\kappa_L^{max}(\lambda,\mu)} c_\kappa(L)|N\hbar\omega(\lambda,\mu)\kappa LM\rangle, \quad (26)$$

where $\kappa_L^{max}(\lambda,\mu)$ denotes the maximum multiplicity of L in (λ,μ), Eq. (7). Obviously, $|\phi_{LM}(N)\rangle$ is an unmixed eigenstate of $H(\beta_0,\beta_2)$ if $\langle\psi(N-2)|\hat{B}_0|\phi_{LM}(N)\rangle=0$ holds for all states $|\psi(N-2)\rangle$ at the $(N-2)\hbar\omega$ level. From the proof it follows that $\hat{B}_0$ acting on states in the "special" irrep (λ,μ) at $N\hbar\omega$ can only produce states belonging to the "special" irrep (λ',μ') at $(N-2)\hbar\omega$, hence $\langle(N-2)\hbar\omega(\lambda',\mu')\kappa' LM|\hat{B}_0|\phi_L(N)\rangle=0$ for $\kappa'=1,2,\ldots,\kappa_L^{max}(\lambda',\mu')$ ensures that $|\phi_{LM}(N)\rangle$ is pure. The $\kappa_L^{max}(\lambda,\mu)$ coefficients $c_\kappa(L)$, which characterize the pure state, are thus uniquely determined by the $\kappa_L^{max}(\lambda',\mu')=\kappa_L^{max}(\lambda,\mu)-1$ equations

$$\sum_\kappa c_\kappa(L)\langle(N-2)\hbar\omega(\lambda',\mu')\kappa' LM|\hat{B}_0|N\hbar\omega(\lambda,\mu)\kappa LM\rangle = 0, \quad (27)$$

and the normalization requirement $\Sigma_\kappa|c_\kappa(L)|^2=1$. The proof given in the preceding section guarantees the existence of a solution.

Making use of the Wigner-Eckart theorem for SU(3) (see Appendix A), the relations in Eq. (27) can be rewritten as

$$\langle(\lambda',\mu')|||B^{(02)}|||(\lambda,\mu)\rangle \times\sum_\kappa c_\kappa(L)\langle(\lambda,\mu)\kappa L;(02)0||(\lambda',\mu')\kappa' L\rangle=0,$$

where $\langle\cdot;\cdot||\cdot\rangle$ denotes a reduced Wigner coupling coefficient for SU(3). Since the triple-reduced matrix element of $B^{(02)}$ is generally nonzero, we obtain the following conditions:

$$\sum_{\kappa=1}^{\kappa_L^{max}(\lambda,\mu)} c_\kappa(L)\langle(\lambda',\mu')\kappa' L;(20)0||(\lambda,\mu)\kappa L\rangle=0 \quad (\kappa'=1,\ldots,\kappa_L^{max}(\lambda,\mu)-1). \quad (28)$$

Note that the matrix elements of the symplectic generators are not relevant for the determination of the $c_\kappa(L)$, and the SU(3) Wigner coefficients, $\langle\cdot;\cdot||\cdot\rangle$, can be evaluated numerically [51] or analytically [53].

To illustrate the procedure outlined above, we consider the case of ^{12}C. The leading irrep for the nucleus is $(\lambda_\sigma,\mu_\sigma)=(0,4)$, thus the pure states belong to $(\lambda,\mu)=(0,4)$ at $0\hbar\omega$, $(\lambda,\mu)=(2,4)$ at $2\hbar\omega$, $(\lambda,\mu)=(4,4)$ at $4\hbar\omega$, etc. At $0\hbar\omega$, all states $(L=0,2,4)$ are unmixed. At $2\hbar\omega$, the possible L values are 0, 2^2, 3, 4^2, 5, 6, and we have $\Delta_{L=0}(2\hbar\omega)=0$ and $\Delta_L(2\hbar\omega)=1$ for $L=2,3,4,5,6$. Since the values $L=3,5,6$ occur only once $(\kappa_L^{max}[(2,4)]=1)$, the associated states are pure $[c_1(L)=1.0]$. For $L=2,4$, for which $\kappa_L^{max}[(2,4)]=2$, the appropriate coefficients $c_\kappa(L)$ may be determined from the requirements

$$c_1(L)\langle(0,4)L;(2,0)0||(2,4)1L\rangle + c_2(L)\langle(0,4)L;(2,0)0||(2,4)2L\rangle=0,$$
$$|c_1(L)|^2+|c_2(L)|^2=1. \quad (29)$$

For $L=2$, one finds $\langle(0,4)2;(2,0)0||(2,4)\kappa 2\rangle=-0.852\,80$ $(0.053\,72)$ for $\kappa=1$ $(\kappa=2)$ [51], and thus $|\phi_{2M}(2\hbar\omega)\rangle = 0.063\ |2\hbar\omega(2,4)12M\rangle + 0.998\ |2\hbar\omega(2,4)22M\rangle$. Similarly, for $L=4$, one obtains $\langle(0,4)4;(2,0)0||(2,4)\kappa 4\rangle = -0.751\,07$ $(0.234\,40)$ for $\kappa=1$ $(\kappa=2)$ [51], and therefore $c_1(4)=0.298$ and $c_2(4)=0.955$. Analogously, one can proceed for the $4\hbar\omega$ level. There are, for instance, three $L=4$ states, one of which is pure. One finds $|\phi_{4M}(4\hbar\omega)\rangle = -0.637\ |4\hbar\omega(4,4)14M\rangle + 0.761\ |4\hbar\omega(4,4)24M\rangle - 0.124\ |2\hbar\omega(4,4)34M\rangle$, and similarly for the other states.

For a nucleus with $(\lambda_\sigma,\mu_\sigma)=(\lambda,0)$, $\lambda>2$, pure states with $(\lambda',\mu')=(\lambda-2,2)$, $L=2,3,\ldots,\lambda-1$, exist at $2\hbar\omega$ according to the proof given in Sec. III. The odd angular momentum values, $L=3,5,\ldots,\lambda-1$, occur only once $(\kappa=1)$ and the associated states are pure. The even-L values, on the other hand, occur twice, with $\kappa=1$ or 2, corresponding to Vergados labels 0 and 2, respectively. Since $\langle(\lambda,0)L;(2,0)0||(\lambda-2,2)\kappa L\rangle=[2(\lambda+1)^2-L(L+1)]^{1/2}/[3\lambda(\lambda+1)]^{1/2}$ for $\kappa=1$ and 0 for $\kappa=2$ [43], it follows that $c_\kappa(L)=0$ (1.0) for $\kappa=1$ $(\kappa=2)$. Consequently, the pure $K=2$ band at $2\hbar\omega$ consists of states with $(\lambda',\mu')=(\lambda-2,2)$, $\kappa=1$ $(\kappa=2)$ for odd (even) L values, i.e., $\kappa=\kappa_L^{max}(\lambda-2,2)$. An example for such a nucleus is given in Sec. V B, where the ^{20}Ne system is discussed.

Having constructed the solvable eigenstates of the PDS Hamiltonian $H(\beta_0,\beta_2)$, Eq. (24), we can now give analytic expressions for their energies. We have $E(N=0)=0$ for the $0\hbar\omega$ level, and

$$E(N)=\beta_2\frac{N}{3}\left(N_\sigma-\lambda_\sigma+\mu_\sigma-6+\frac{3}{2}N\right)\quad(\lambda_\sigma>\mu_\sigma),$$
$$E(N)=\beta_2\frac{N}{3}\left(N_\sigma+2\lambda_\sigma+\mu_\sigma-3+\frac{3}{2}N\right)\quad(\lambda_\sigma\leqslant\mu_\sigma), \quad (30)$$

for $N>0$. For instance, for $N_\sigma(\lambda_\sigma,\mu_\sigma)=24.5$ (0,4), which corresponds to ^{12}C, this yields $E(N=0)=0$, $E(2\hbar\omega)=19\beta_2$, $E(4\hbar\omega)=42\beta_2$, etc.

The partial SU(3) symmetry of $H(\beta_0,\beta_2)$ is converted into partial dynamical SU(3) symmetry by adding to the Hamiltonian SO(3) rotation terms that lead to $L(L+1)$-type splitting but do not affect the wave functions. The solvable states then form rotational bands and since their wave functions are known, one can evaluate the quadrupole transition rates between them,

$$B(E2,L_i\to L_f)=e^2b^4\left(\frac{Z}{A}\right)^2\frac{5}{16\pi}\frac{|\langle L_f||Q_2||L_i\rangle|^2}{2L_i+1}. \quad (31)$$

Here $b=\sqrt{\hbar/m\omega}$ is the harmonic oscillator length parameter, Z and A are the nuclear charge and mass, respectively, and the convention for the reduced matrix elements is summarized in Appendix A. For unmixed initial and final states, $|\phi_{L_i}(N_i)\rangle=\Sigma_{\kappa_i}c_{\kappa_i}(L_i)|N_i\hbar\omega(\lambda_i,\mu_i)\kappa_iL_i\rangle$ and $|\phi_{L_f}(N_f)\rangle=\Sigma_{\kappa_f}c_{\kappa_f}(L_f)|N_f\hbar\omega(\lambda_f,\mu_f)\kappa_fL_f\rangle$, the matrix element of Q_2 is given by

$$\begin{aligned}\langle\phi_{L_f}(N_f)||Q_2||\phi_{L_i}(N_i)\rangle &= \delta_{N_i,N_f}\delta_{(\lambda_i,\mu_i)(\lambda_f,\mu_f)}(-1)^{\phi_{\mu_i}}\sqrt{6\langle C_{SU(3)}\rangle[(\lambda_i,\mu_i)]}\sum_{\kappa_i\kappa_f}c_{\kappa_i}(L_i)c_{\kappa_f}(L_f)\langle(\lambda_i,\mu_i)\kappa_iL_i;(11)2||(\lambda_i,\mu_i)\kappa_fL_f\rangle_{\rho=1}\\ &+\delta_{N_i,(N_f+2)}\sqrt{3}\langle(\lambda_f,\mu_f)|||A^{(20)}|||(\lambda_i,\mu_i)\rangle\sum_{\kappa_i\kappa_f}c_{\kappa_i}(L_i)c_{\kappa_f}(L_f)\langle(\lambda_i,\mu_i)\kappa_iL_i;(20)2||(\lambda_f,\mu_f)\kappa_fL_f\rangle\\ &+\delta_{N_i,(N_f-2)}\sqrt{3}\langle(\lambda_f,\mu_f)|||B^{(02)}|||(\lambda_i,\mu_i)\rangle\sum_{\kappa_i\kappa_f}c_{\kappa_i}(L_i)c_{\kappa_f}(L_f)\langle(\lambda_i,\mu_i)\kappa_iL_i;(02)2||(\lambda_f,\mu_f)\kappa_fL_f\rangle, \quad (32)\end{aligned}$$

where $\phi_\mu=0$ for $\mu=0$ and 1 otherwise.

For intraband transitions, the above expression reduces to the first term on the right-hand side. For interband transitions there are three possibilities: For transitions from $N\hbar\omega$ to $(N+2)\hbar\omega$, the second term has to be evaluated; for $N\hbar\omega\to(N-2)\hbar\omega$ transitions, the third term is required; for $\lambda_\sigma\neq0$, $\mu_\sigma\neq0$, i.e., for triaxially deformed nuclei, a $N=0\to N=0$ transition is possible as well; in that case the relevant contribution originates from the first term. For example, for a transition from $L_i=2$ to $L_f=0$ in the ground band of ^{12}C, $b=1.668$ fm, $6\langle\hat{C}_{SU(3)}\rangle[(0,4)]=112$, and thus $B(E2,0\hbar\omega L_i=2\to0\hbar\omega L_f=0)=0.1925\ e^2\mathrm{fm}^4\times112|\langle(0,4)2;(1,1)2||(0,4)0\rangle|^2/5=4.31\ e^2\mathrm{fm}^4=2.64$ W.u. (Weisskopf units) (which corresponds to 4.65 W.u., when an effective charge $e^*=1.327$ is used).

V. APPLICATIONS TO LIGHT NUCLEI

To illustrate that the PDS Hamiltonians of Eq. (24) are physically relevant, we present applications to prolate, oblate, and triaxially deformed nuclei. We compare energy

TABLE I. $B(E2)$ values (in Weisskopf units) for ground band transitions in ^{12}C. Compared are several symplectic calculations, PDS results, and experimental data. Q denotes the static quadrupole moment of the $L^\pi=2_1^+$ state and is given in units of eb. The experimental values are taken from Refs. [52,55]. PDS results are rescaled by an effective charge $e^*=1.33$ and the symplectic calculations employ bare charges.

Transition	Model $B(E2)$ (W.u.)					$B(E2)$ (W.u.)
$J_i \to J_f$	$2\hbar\omega$	$4\hbar\omega$	$6\hbar\omega$	$8\hbar\omega$	PDS	Expt.
$2\to 0$	4.65	4.65	4.65	4.65	4.65	4.65 ± 0.26
$4\to 2$	4.35	4.27	4.24	4.23	4.28	n/a
Q (eb)	0.059	0.060	0.060	0.060	0.058	0.06 ± 0.03

spectra, reduced quadrupole transition rates, and eigenstates of

$$H_{PDS}=h(N)+\xi H(\beta_0=12,\beta_2=18)+\gamma_2\hat{L}^2+\gamma_4\hat{L}^4, \tag{33}$$

to those of the symplectic Hamiltonian

$$H_{\mathrm{Sp(6)}}=\hat{H}_0-\chi Q_2\cdot Q_2+d_2\hat{L}^2+d_4\hat{L}^4. \tag{34}$$

Here the function $h(N)$, which contains the harmonic oscillator term $\hat{H}_0$, is simply a constant for a given $N\hbar\omega$ excitation. We select light, p shell and ds shell, nuclei for which a full, three-dimensional symplectic calculation can be carried out, that is, a limitation to a submodel of the Sp(6,R) model is not required. Since we employ Hamiltonians composed solely of sp(6,R) generators, we restrict the model space to one sp(6,R) irrep (represented by one ''cone'' in Fig. 2). We include excitations up to $8\hbar\omega$.

A. The ^{12}C case

The first nucleus to be considered is ^{12}C, with four protons and four neutrons in the valence p shell. This nucleus has previously been studied in the Sp(2,R) submodel of the SSM [33,54]. Here we employ the full, three-dimensional, symplectic shell model. The leading sp(6,R) irrep for this case is $N_\sigma(\lambda_\sigma,\mu_\sigma)=24.5(0,4)$. At the $2\hbar\omega$ level SU(3) irreps $(\lambda,\mu)=(2,4)$, (1,3), (0,2) occur, at the $4\hbar\omega$ level we have $(\lambda,\mu)=(0,6)$, (1,4), $(2,2)^2$, (4,4), (3,3), (1,1), (0,0), and so on for higher excitations. The parameters of $H_{\mathrm{Sp(6)}}$ were fitted (simultaneously) to the ground band energies and the $2_1^+\to 0_1^+$ reduced quadrupole transition strength, for symplectic model spaces including excitations up to $2\hbar\omega$, $4\hbar\omega$, $6\hbar\omega$, and $8\hbar\omega$. The resulting $B(E2)$ strengths are listed in Table I and several low-lying rotational bands are shown in Fig. 3. The left part of the figure shows the experimental energies of the ground band [55], while the center portion (labeled $Q_2\cdot Q_2$) shows the calculated ground band ($K=0_1$), as well as several resonance bands that are dominated by $2\hbar\omega$ excitations ($K=2_1,0_2,1_1,0_3$), $4\hbar\omega$ excitations ($K=4_1$), and $6\hbar\omega$ excitations ($K=6_1$). The parameters of H_{PDS} were determined as follows: γ_2 and γ_4 were fixed by the level splittings of the ground band, ξ was chosen to fit the

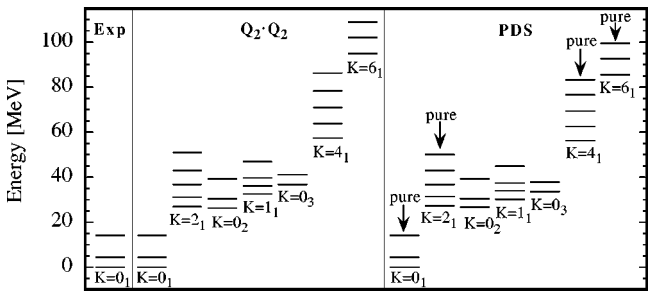

FIG. 3. Energy spectra for ^{12}C. Comparison between experimental values (left) [55], results from a symplectic $8\hbar\omega$ calculation (center) and a PDS calculation (right). $K=0_1$ indicates the ground band in all three parts of the figure. In addition, resonance bands dominated by $2\hbar\omega$ excitations ($K=2_1,0_2,1_1,0_3$), $4\hbar\omega$ excitations ($K=4_1$), and $6\hbar\omega$ excitations ($K=6_1$) are shown for the Sp(6,R) and PDS calculations. Additional mixed resonance bands (not shown), dominated by $4\hbar\omega$ and $6\hbar\omega$ excitations, exist for this nucleus. The angular momenta of the positive parity states in the rotational bands are $L=0,2,4,\ldots$ for $K=0$ and $L=K,K+1,K+2,\ldots$ otherwise. Bands that consist of pure-SU(3) eigenstates of the PDS Hamiltonian are indicated.

energy difference between the $K=2_1$ and $K=0_2$ bandheads of the symplectic calculation, and $h(N)$ was adjusted to reproduce approximately the relative positions of the $K=0_1,2_1,4_1$, and 6_1 bandheads. The resulting spectrum is that shown on the right side of Fig. 3, labeled PDS.

Since H_{PDS} does not mix states with different $N\hbar\omega$ excitations, the $B(E2)$ values obtained in the PDS calculations require an effective charge $e^*=1.33$ to match the experimental values [55] (compare Table I). Overall, we find little deviation between the energies and electromagnetic transition strengths of the two approaches. A better measure for the level of agreement between the PDS and symplectic results is given by a comparison of the eigenstates. According to the proof given in Sec. III, the Hamiltonian H_{PDS} should have sets of solvable, pure-SU(3) eigenstates, which can be organized into rotational bands: All $0\hbar\omega$ states should be pure $(\lambda_\sigma,\mu_\sigma)=(0,4)$ states, and at $2\hbar\omega$ a rotational band with good SU(3) symmetry $(\lambda,\mu)=(2,4)$ and $L=2,3,4,5,6$ should exist. Similarly, we expect pure-SU(3) bands at $4\hbar\omega$ with $(\lambda,\mu)=(4,4)$ and $L=4,5,6,7,8$, at $6\hbar\omega$ with $(\lambda,\mu)=(6,4)$ and $L=6,7,8,9,10$, etc. An analysis of the PDS eigenstates shows that this is indeed the case. The associated rotational bands are indicated in Fig. 3.

Figure 4 shows the decomposition of representative ($L^\pi=2^+$) states of the five lowest rotational bands for the $H_{\mathrm{Sp(6)}}$ and H_{PDS} Hamiltonians. The left side of the figure illustrates the amount of mixing in the wave functions of the $8\hbar\omega$ ($Q_2\cdot Q_2$) calculation: Members of the ground band ($K=0_1$) are nearly pure ($\approx 90\%$) $0\hbar\omega$ states and the resonance bands have strong $2\hbar\omega$ contributions ($\geqslant 60\%$). The $K=2_1$, 1_1, and 0_3 bands contain admixtures from $N\hbar\omega$ excited states with $N>2$, while the $K=0_2$ contains admixtures from both the $0\hbar\omega$ space and from higher oscillator shells. The relative strengths of the SU(3) irreps within the $2\hbar\omega$ space are given as well. We find that each rotational band tends to be dominated by one representation, namely, (2,4)

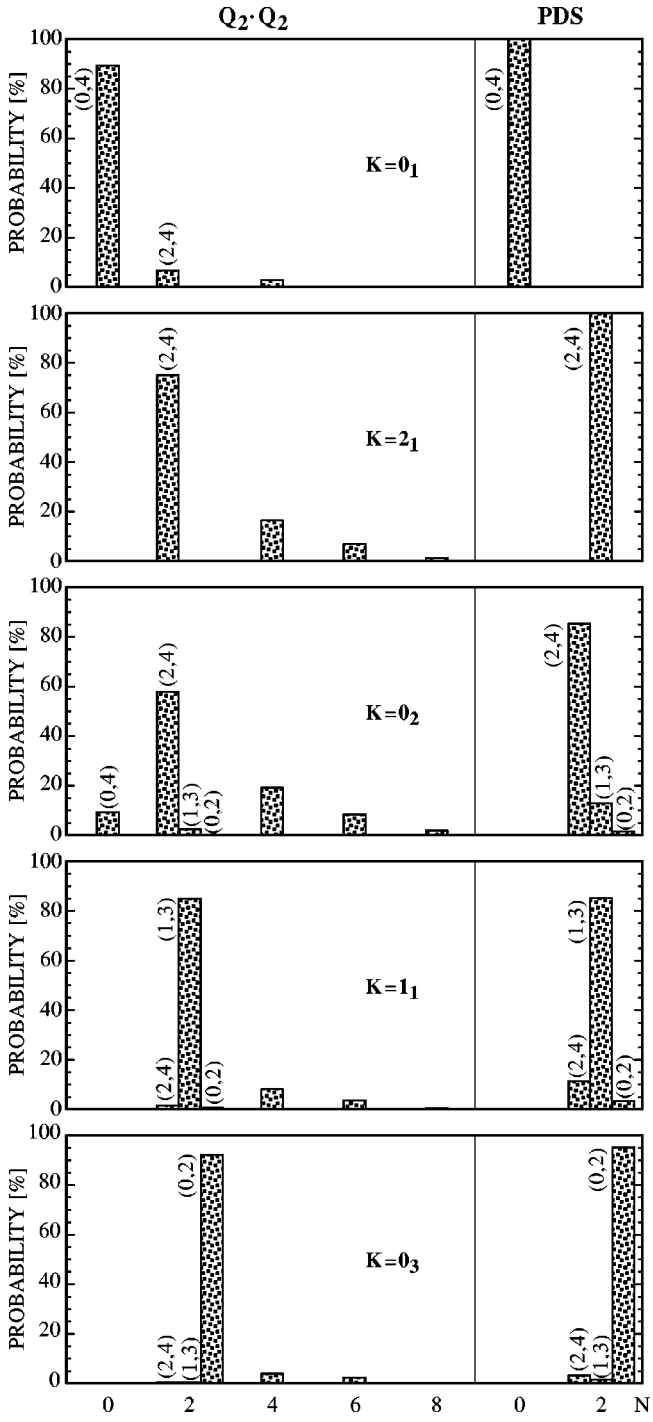

FIG. 4. Decompositions for calculated $L^{\pi}=2^{+}$ states of ^{12}C. Individual contributions from the relevant SU(3) irreps at the $0\hbar\omega$ and $2\hbar\omega$ levels are shown for both a symplectic $8\hbar\omega$ calculation (denoted $Q_2\cdot Q_2$) and a PDS calculation. In addition, the total strengths contributed by the $N\hbar\omega$ excitations for $N>2$ are given for the symplectic case.

for the $K=2_1$ and $K=0_2$ bands, (1,3) for $K=1_1$, and (0,2) for $K=0_3$, with the other irreps contributing less than 3%. The right side of Fig. 4 shows the structure of the PDS eigenstates. Since the Hamiltonian H_{PDS} does not mix different major oscillator shells, each eigenstate belongs entirely to one $N\hbar\omega$ level of excitation. Here the ground band belongs

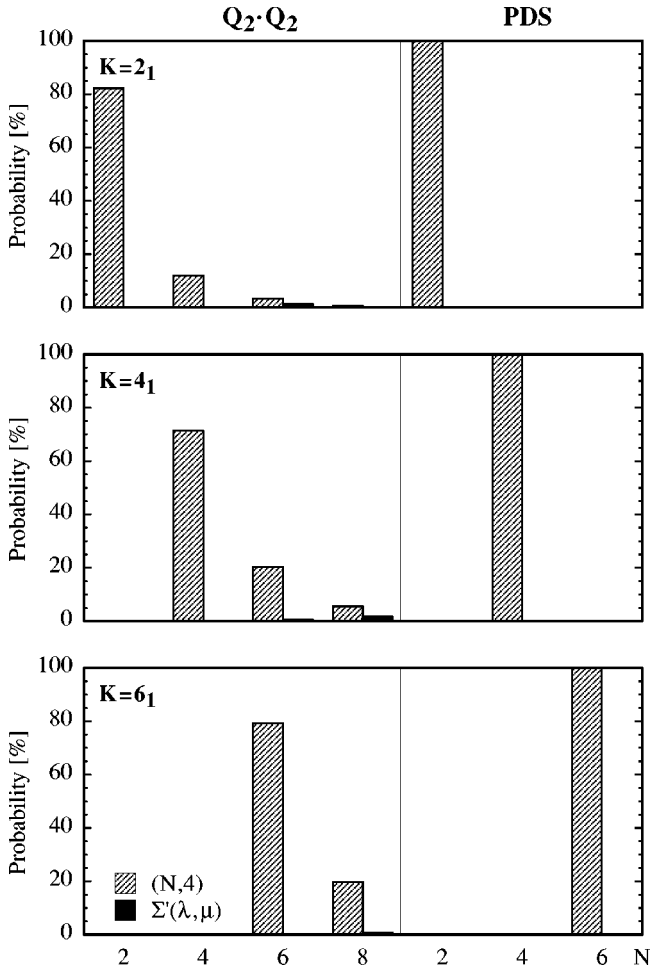

FIG. 5. Decompositions for calculated $L^{\pi}=6^{+}$ states of ^{12}C. The structures shown are representative for the members of the $K=2_1$, 4_1, and 6_1 rotational bands, respectively. States of these bands are dominated by $N\hbar\omega$ excited configurations with $(\lambda,\mu)=(N,4)$, $N=2,4,6,8$, in the symplectic scheme and are pure in the PDS approach.

to the $0\hbar\omega$ space, while the four resonance bands are pure $2\hbar\omega$ configurations. Comparing this with the symplectic results, we observe that the $N\hbar\omega$ level to which a particular PDS band belongs also dominates the corresponding symplectic band. Furthermore, within this dominant excitation, eigenstates of $H_{\mathrm{Sp}(6)}$ and H_{PDS} have very similar SU(3) structure, that is, the relative strengths of the various SU(3) irreps in the symplectic states are approximately reproduced in the PDS case. This holds for the $K=0_1$ and $K=2_1$ bands, which are pure in the PDS scheme, as well as for the mixed $K=0_2$, 1_1, and 0_3 bands. The above statements are also true for higher $N\hbar\omega$ excitations, as is illustrated in Fig. 5 for the $L=6$ states of the $N=2$, $K=2_1$; $N=4$, $K=4_1$; and $N=6$, $K=6_1$ bands. Note also that, in the symplectic case, admixtures from higher shells in the $L=6$ wave functions originate predominantly from the ''special'' irreps $(\lambda,\mu)=(N,4)$.

The ^{12}C example given above nicely illustrates the concept of a partial dynamical symmetry for a fermionic many-body system. The pure PDS eigenstates form rotational

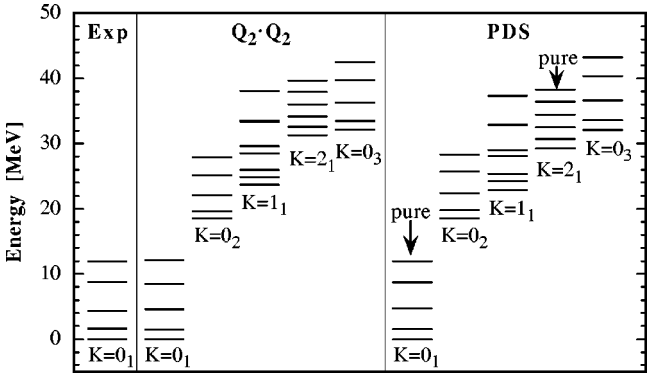

FIG. 6. Energy spectra for ^{20}Ne. Experimental ground band ($K=0_1$) energies [60] are shown on the left, while theoretical results for both the ground band and $2\hbar\omega$ resonances ($K=0_2,1_1,2_1,0_3$) are given in the center and on the right, for a symplectic $8\hbar\omega$ and a PDS calculation, respectively. Rotational bands that consist of pure eigenstates of the PDS Hamiltonian are indicated.

bands that follow the pattern for solvable states of family (b), their energies and $E2$ transition strengths between them can be evaluated analytically according to Eqs. (30)–(32).

B. The ^{20}Ne case

We now turn to a system with pure PDS eigenstates that follow pattern (a): The ^{20}Ne nucleus, with two valence protons and neutrons each, has previously been described within the symplectic model framework [29,47,58,59]. The leading sp(6,R) irrep for this prolate nucleus is $N_\sigma(\lambda_\sigma,\mu_\sigma)=48.5(8,0)$. We expect to find solvable, pure-SU(3) eigenstates of H_{PDS} at $0\hbar\omega$, $2\hbar\omega$, and $4\hbar\omega$. More specifically, there should be a $K=0_1$, $L=0,2,4,6,8$ rotational band with $(\lambda,\mu)=(8,0)$ at $0\hbar\omega$, a $K=2_1$, $L=2,3,4,5,6,7$ band with $(\lambda,\mu)=(6,2)$ at $2\hbar\omega$, and a $K=4_1$, $L=4,5$ "band" with $(\lambda,\mu)=(4,4)$ at $4\hbar\omega$. Pure PDS states at higher levels of excitation do not exist.

As in the ^{12}C case, we compare the eigenstates of H_{PDS} to those of the symplectic Hamiltonian $H_{\mathrm{Sp}(6)}$. Least squares fits to measured energies and $B(E2)$ values of the ground band of ^{20}Ne [60] were carried out for $2\hbar\omega$, $4\hbar\omega$, $6\hbar\omega$, and $8\hbar\omega$ symplectic model spaces. The resulting energies and transition rates converge to values that agree with the data, as is illustrated in Fig. 6 and Table II. The parameters γ_2 and γ_4 in H_{PDS} were determined by the energy splitting between states of the ground band, ξ was adjusted to reproduce the relative positions of the $2\hbar\omega$ resonance bandheads and $h(N)$ was fixed by the energy difference $[E(0_2^+)-E(0_1^+)]$. Figure 6 and Table II demonstrate the level of agreement between the PDS and symplectic results.

An analysis of the structure of the ground and resonance bands reveals the amount of mixing in the $8\hbar\omega$ symplectic $(Q_2\cdot Q_2)$ wave functions. Figure 7 shows the decomposition for representative $(L^\pi=2^+)$ states of the five lowest rotational bands. Ground band $(K=0_1)$ states are found to have a strong $0\hbar\omega$ component ($\geqslant 64\%$), and three of the four resonance bands are clearly dominated ($\geqslant 60\%$) by $2\hbar\omega$ configurations. States of the first resonance band $(K=0_2)$, however, contain significant contributions from all but the highest $N\hbar\omega$ excitations. The relative strengths of the SU(3) irreps within the $2\hbar\omega$ space are shown as well. As in the ^{12}C case, states are found to be dominated by one representation [(10,0) for the $K=0_2$ band, (8,1) for $K=1_1$, (6,2)$\kappa=2$ for $K=2_1$, and (6,2)$\kappa=1$ for $K=0_3$ here], while the other irreps contribute only a few percent. Such trends are present also in the more realistic symplectic calculations of Suzuki [59].

TABLE II. $B(E2)$ values (in Weisskopf units) for ground band transitions in ^{20}Ne. Compared are experimental data, predictions from several symplectic calculations, and PDS results. The static quadrupole moment of the $L^\pi=2_1^+$ state is given in the last row. The experimental values are taken from Refs. [56,57,60]. PDS transition rates are rescaled by an effective charge $e^*=1.95$, while the symplectic calculations use bare charges.

Transition	Model $B(E2)$ (W.u.)					$B(E2)$ (W.u.)
$J_i\rightarrow J_f$	$2\hbar\omega$	$4\hbar\omega$	$6\hbar\omega$	$8\hbar\omega$	PDS	Expt.
$2\rightarrow 0$	14.0	18.7	19.1	19.3	20.3	20.3 ± 1.0
$4\rightarrow 2$	18.4	24.5	24.6	24.5	25.7	22.0 ± 2.0
$6\rightarrow 4$	17.1	22.3	21.5	20.9	21.8	20.0 ± 3.0
$8\rightarrow 6$	12.4	15.2	13.3	12.4	12.9	9.0 ± 1.3
Q (eb)	-0.14	-0.16	-0.16	-0.16	-0.17	-0.23 ± 0.03

As expected, H_{PDS} has families of pure-SU(3) eigenstates that can be organized into rotational bands, Fig. 6. The ground band belongs entirely to $N=0$, $(\lambda,\mu)=(8,0)$, and all states of the $K=2_1$ band have quantum labels $N=2$, $(\lambda,\mu)=(6,2)$, $\kappa=2$. The $K=4_1$ band at $4\hbar\omega$ is not shown. A comparison with the symplectic case shows that the $N\hbar\omega$ level to which a particular PDS band belongs is also dominant in the corresponding symplectic band, Fig. 7. As before, within this dominant excitation, eigenstates of H_{PDS} and $H_{\mathrm{Sp}(6)}$ have similar SU(3) distributions; in particular, both Hamiltonians favor the same $(\lambda,\mu)\kappa$ values. Significant differences in the structure of the wave functions appear, however, for the $K=0_2$ resonance band. In the $8\hbar\omega$ symplectic calculation, this band contains almost equal contributions from the $0\hbar\omega$, $2\hbar\omega$, and $4\hbar\omega$ levels, with additional admixtures of $6\hbar\omega$ and $8\hbar\omega$ configurations, while in the PDS calculation, it belongs entirely to the $2\hbar\omega$ level. These structural differences are also evident in the interband transition rates, as is illustrated in Table III. Whereas the intraband $B(E2)$ strengths are approximately equal in both approaches, we observe that the interband rates differ by a factor of 2–3 in most cases. These differences reflect the action of the intershell coupling terms that are present in the quadrupole-quadrupole interaction of Eq. (23), but do not occur in the PDS Hamiltonian. Increasing the strength χ of $Q_2\cdot Q_2$ in $H_{\mathrm{Sp}(6)}$ will also spread the other resonance bands over many $N\hbar\omega$ excitations. The $K=2_1$ band (which is pure in the PDS scheme) is found to resist this spreading more strongly than the other resonances. For physically relevant values of χ, the low-lying bands have the structure shown in Fig. 7.

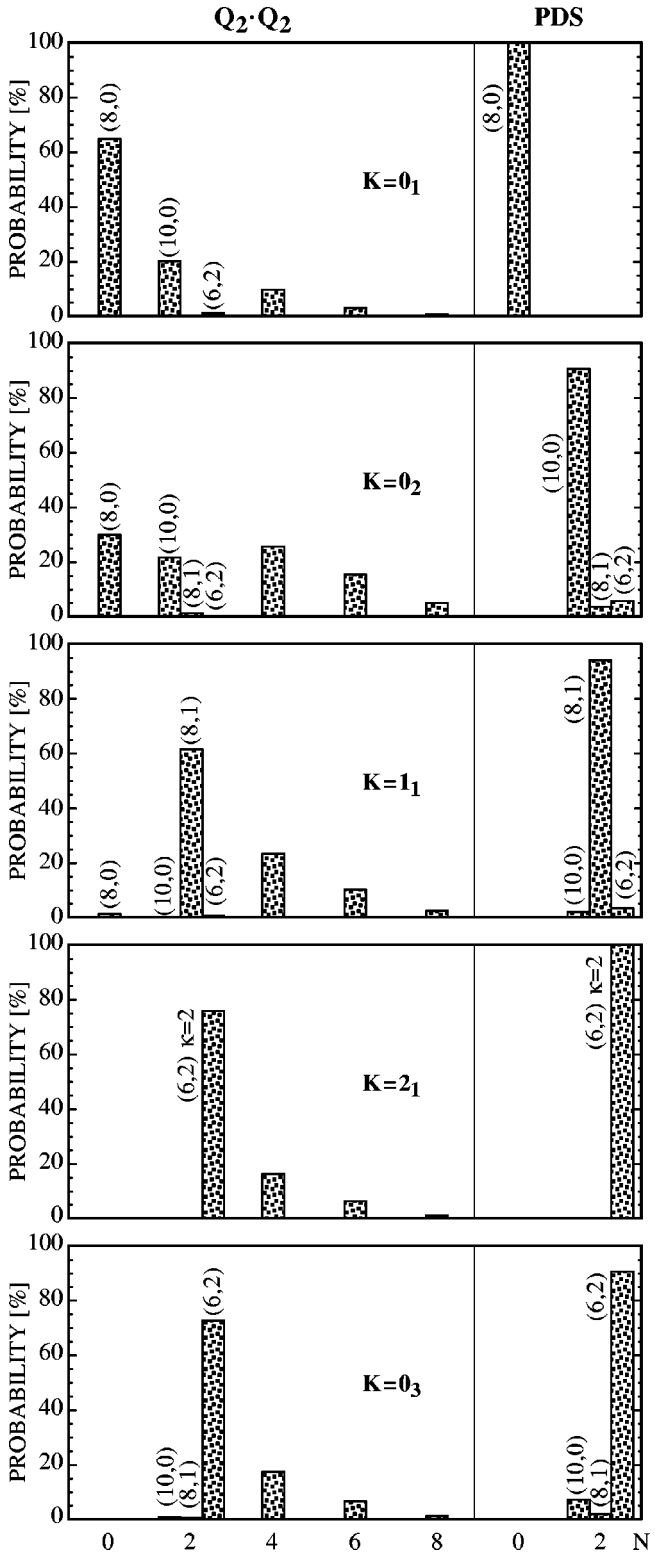

FIG. 7. Decompositions for calculated $L^{\pi}=2^{+}$ states of ^{20}Ne. Individual contributions from the SU(3) irreps at the $0\hbar\omega$ and $2\hbar\omega$ levels are shown for both a symplectic $8\hbar\omega$ calculation (left side) and a PDS calculation (right side). For the symplectic approach the summed contributions from SU(3) irreps at higher ($N>2$) excitations are given as well.

TABLE III. Comparison of intraband and interband $B(E2)$ rates for ^{20}Ne. Shown are various transitions between states of the lowest rotational bands. $K=0_1$ denotes the ground band, which is dominated by $0\hbar\omega$ configurations; members of the other bands correspond to $2\hbar\omega$ resonances. Results are from the PDS calculation (rescaled by $e^*=1.95$) and from the $8\hbar\omega$ symplectic approach ($e^*=1.0$). In the last column, ratios of the calculated transition strengths are given.

Transition				Model $B(E2)$ (W.u.)		$\frac{B(E2)[\mathrm{PDS}]}{B(E2)[\mathrm{Sp6}]}$
J_i	K_i	J_f	K_f	Sp(6,R)	PDS	
2	0_1	0	0_1	19.3	20.3	1.05
2	0_2	0	0_1	5.8	12.6	2.16
2	0_3	0	0_1	0.10	0.32	3.16
2	0_1	0	0_2	2.9	5.7	1.94
2	0_2	0	0_2	20.3	27.8	1.37
2	0_3	0	0_2	0.15	0.13	0.84
2	0_1	0	0_3	0.17	0.48	2.80
2	0_2	0	0_3	0.25	0.26	1.01
2	0_3	0	0_3	12.9	16.8	1.30
4	0_1	2	0_1	24.5	25.7	1.05
4	0_2	2	0_1	10.9	22.8	2.09
4	1_1	2	0_1	2.3	5.8	2.55
4	2_1	2	0_1	0.63	2.3	3.66
4	0_3	2	0_1	0.09	0.30	3.34

C. The ^{24}Mg case

The final example to be considered here involves the triaxially deformed nucleus ^{24}Mg, which has been the subject of several symplectic model studies [46,47,61,62]. With four valence protons and neutrons in the *ds* shell each, and a leading sp(6,R) irrep $N_\sigma(\lambda_\sigma,\mu_\sigma)=62.5(8,4)$, this system is the most complicated one to be investigated here. Since both $\lambda_\sigma\neq 0$ and $\mu_\sigma\neq 0$, the symplectic Hilbert space has a very rich structure. The (8,4) representation at $0\hbar\omega$ contains three rotational bands: a $K=0$ band with $L=0,2,4,6,8$; a $K=2$ band with $L=2,3,\ldots,10$; and a $K=4$ band with $L=4,5,\ldots,12$. At the $2\hbar\omega$ level, there are six possible SU(3) irreps, (10,4), (8,5), (6,6), (9,3), (7,4), and (8,2), which contain a total of four $K=0$, two $K=1$, four $K=2$, two $K=3$, three $K=4$, one $K=5$, one $K=6,\ldots$ bands. At the $4\hbar\omega$ level, there are 15 different SU(3) irreps, at $6\hbar\omega$, there are 25, etc. Accordingly, the number of states for a given angular momentum value L increases dramatically with the inclusion of higher excitations. This is illustrated in Table IV for L

TABLE IV. Dimensions of symplectic Hilbert spaces for ^{24}Mg. Shown are the number of L states ($L=0,1,\ldots,8$) for spaces that include $N\hbar\omega$ excitations up to $N=0$, 2, 4, and 6, respectively.

Symplectic	Angular momentum L								
space	0	1	2	3	4	5	6	7	8
$0\hbar\omega$	1	0	2	1	3	2	3	2	3
$(0+2)\hbar\omega$	4	3	11	10	17	15	19	16	18
$(0+2+4)\hbar\omega$	13	15	40	41	62	59	71	63	67
$(0+2+4+6)\hbar\omega$	32	49	110	122	171	171	198	182	187

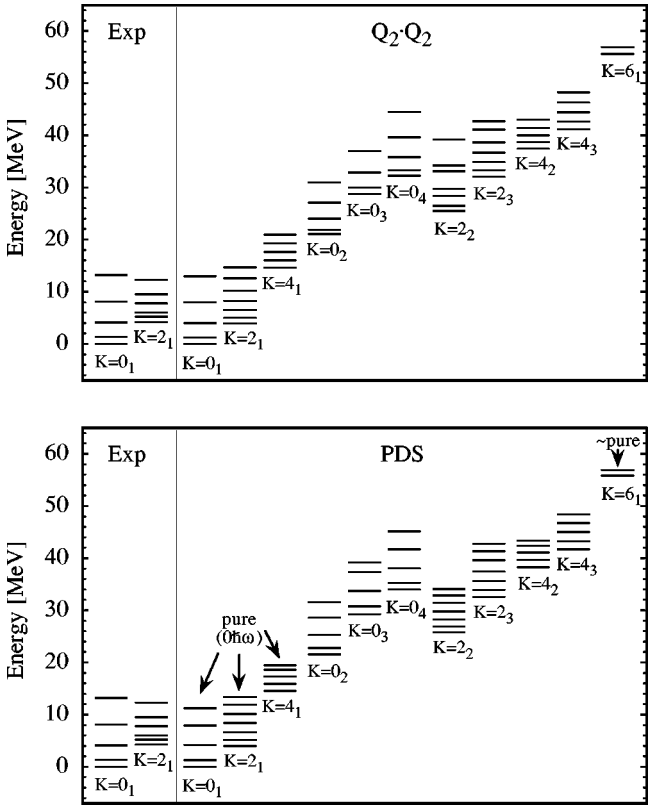

FIG. 8. Energy spectra for ^{24}Mg. Energies from a PDS calculation (bottom) are compared to symplectic results (top). Both $0\hbar\omega$-dominated bands ($K=0_1,2_1,4_1$) and some $2\hbar\omega$ resonance bands ($K=0_2,0_3,0_4,2_2,2_3,4_2,4_3,6_1$) are shown. The $K=0_1,2_1,4_1$ (6_1) states are pure (approximately pure) in the PDS scheme. Experimental values for the ground and γ-band energies, taken from Refs. [63,64], are given on the left.

$=0,1,2,\ldots,8$.

Since the interactions in $H_{\mathrm{Sp}(6)}$ do not distinguish different κ multiplicities, it becomes necessary to make use of the integrity basis operators $\hat{X}_3$ and $\hat{X}_4$ discussed in Sec. II, which allow us to reproduce the experimentally observed K band splitting in the spectrum of ^{24}Mg. Using the Hamiltonian

$$H'_{\mathrm{Sp}(6)}=H_{\mathrm{Sp}(6)}+c_3\hat{X}_3+c_4\hat{X}_4, \tag{35}$$

we carried out least squares fits to measured energies and $B(E2)$ values for $2\hbar\omega$, $4\hbar\omega$, and $6\hbar\omega$ symplectic spaces.

Figure 8 (top) displays the energies obtained with the $6\hbar\omega$ calculation (right part of the figure) in comparison with the experimental values [63,64] (left side). In addition to the ground ($K=0_1$) and γ ($K=2_1$) bands, the calculated $K=4_1$ band, which is dominated by $0\hbar\omega$ configurations, and several low-lying symplectic $K=0$, 2, 4, and 6 bands, which are dominantly $2\hbar\omega$ resonances, are shown. Table V lists various $B(E2)$ transition rates between the low-lying states of ^{24}Mg. We find that the results of the symplectic calculations are in good agreement with the data [65]. Specifically, the γ band is correctly located and nearly all the calculated intraband and interband transition rates fall, without the use of an effective charge, within experimental uncertainties. The $4\hbar\omega$ results are better than the $2\hbar\omega$ results, with the $6\hbar\omega$ calculation yielding only moderate improvements.

TABLE V. $B(E2)$ strengths of ^{24}Mg. Compared are results from $2\hbar\omega$, $4\hbar\omega$, and $6\hbar\omega$ symplectic calculations, a PDS calculation, and experiment [57,63]. Both intraband and interband transitions between states of the ground ($K=0_1$) and γ ($K=2_1$) band are given. The static quadrupole moment of the 2_1^+ state is listed in the last line (in units of eb). (Measurements have given results for $|Q|$ ranging from less than 0.16 eb to nearly double that value. We list the value adopted in the review by Spear [57].) The symplectic model reproduces the observed transition rates without employing effective charges, while the PDS approach requires $e^*=1.75$.

Transition				Model $B(E2)$				$B(E2)$
J_i	K_i	J_f	K_f	$2\hbar\omega$	$4\hbar\omega$	$6\hbar\omega$	PDS	Expt.
2	0_1	0	0_1	17.2	20.2	20.4	20.5	20.5 ± 0.6
4	0_1	2	0_1	24.5	26.9	26.9	26.2	23 ± 4
6	0_1	4	0_1	25.2	25.5	25.2	22.5	34^{+36}_{-10}
8	0_1	6	0_1	24.4	19.4	19.2	13.6	16^{+25}_{-6}
3	2_1	2	2_1	31.6	35.6	35.3	36.6	34 ± 6
4	2_1	2	2_1	9.7	11.2	11.0	11.6	16 ± 3
5	2_1	3	2_1	15.3	17.0	16.6	16.8	28 ± 5
5	2_1	4	2_1	17.3	18.0	17.7	18.0	14 ± 6
6	2_1	4	2_1	15.3	19.4	18.3	20.1	23^{+23}_{-8}
8	2_1	6	2_1	12.4	18.0	15.9	19.6	$\geqslant3$
2	2_1	0	0_1	1.1	1.3	1.3	3.1	1.4 ± 0.3
2	2_1	2	0_1	2.2	1.7	1.9	3.4	2.7 ± 0.4
3	2_1	2	0_1	1.9	2.4	2.3	5.6	2.1 ± 0.3
4	2_1	2	0_1	0.2	1.0	0.9	2.7	1.0 ± 0.2
4	2_1	4	0_1	2.9	2.1	2.3	4.1	1.0 ± 1.0
5	2_1	4	0_1	1.0	2.4	2.0	6.0	3.9 ± 0.8
6	2_1	4	0_1	0.2	1.2	1.0	3.2	$0.8^{+0.8}_{-0.3}$
	Q (eb)			-0.171	-0.186	-0.185	-0.191	-0.18 ± 0.02

In analogy with the symplectic case, we include terms $\hat{X}_3$ and $\hat{X}_4$ in the PDS Hamiltonian,

$$H'_{PDS}=H_{PDS}+c_3\hat{X}_3+c_4\hat{X}_4. \tag{36}$$

As we will see below, the introduction of these extra terms breaks the partial symmetry. We fixed c_3 and c_4 at the values that were used in the $6\hbar\omega$ symplectic calculation, determined γ_2 and γ_4 from the level splittings in the $K=0_1$ ground band, and adjusted ξ so as to reproduce the relative positions of selected $2\hbar\omega$ bandhead states (we focused on the lowest three $K=0$ bands and the first $K=6$ band). Then $h(N)$ was chosen to reproduce approximately the positions of the $2\hbar\omega$ resonances relative to the ground and γ bands.

We obtain an energy spectrum that agrees well with the results of the symplectic calculation, as is shown in Fig. 8. The $B(E2)$ strengths for the ground and γ bands, rescaled by an effective charge $e^*=1.75$, are given in Table V. We find good agreement between the PDS and symplectic calculations for the intraband transitions, whereas there are larger deviations in the interband rates.

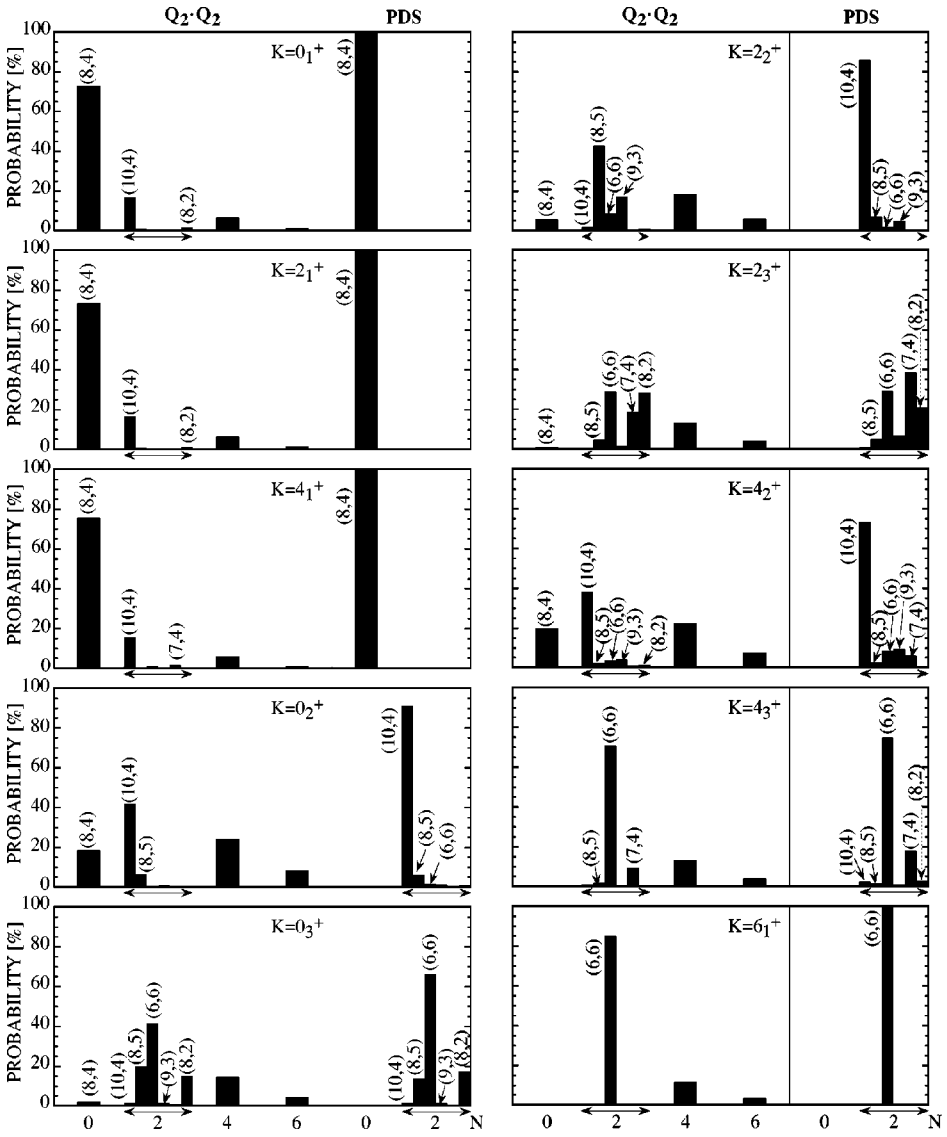

FIG. 9. Decompositions for calculated $L^{\pi}=6^{+}$ states of ^{24}Mg. Eigenstates resulting from the symplectic $6\hbar\omega$ calculation are decomposed into their $0\hbar\omega$, $2\hbar\omega$, $4\hbar\omega$, and $6\hbar\omega$ components (denoted by $Q_2\cdot Q_2$ in the figure). At the $0\hbar\omega$ and $2\hbar\omega$ levels, contributions from the individual SU(3) irreps are shown, for higher excitations ($N>2$) only the summed strengths are given. Eigenstates of the PDS Hamiltonian belong entirely to one $N\hbar\omega$ level of excitation, here $0\hbar\omega$ or $2\hbar\omega$. Contributions from the individual SU(3) irreps at these levels are shown. Members of the $K=0_1,2_1,4_1$ bands are pure in the PDS scheme, and $K=6_1$ states are nearly ($>99\%$) pure.

According to the proof given in Sec. III, the three rotational bands at $0\hbar\omega$ should be pure in the PDS scheme, and at $2\hbar\omega$ there should be a (short) rotational $K=6$ band with $L=6,7$, which belongs entirely to the $(\lambda,\mu)=(6,6)$ representation. We find that the $0\hbar\omega$ states are indeed pure, but the $K=6$, $L=6,7$ band has small admixtures ($<1\%$) from $2\hbar\omega$ irreps other than $(\lambda,\mu)=(6,6)$, thus indicating that H'_{PDS}, unlike H_{PDS}, is not an exact partial dynamical symmetry Hamiltonian, due to the presence of the K-band splitting terms $\hat{X}_3$ and $\hat{X}_4$. This can be understood as follows: While $\hat{X}_3$ and $\hat{X}_4$ cannot mix different SU(3) irreps, their eigenstates involve particular linear combinations of different κ values. Since the operators $\hat{X}_3$ and $\hat{X}_4$ do not commute with $\hat{B}_0$, these linear combinations differ from configurations resulting from the PDS requirement $\hat{B}_0|\phi\rangle=0$. Fortunately, a very small amount of symmetry breaking suffices to fit the relative positions of the ground and γ bands, as can be inferred from the eigenstate decompositions plotted in Fig. 9. Shown are the decompostions of the $L=6$ states associated with the calculated $H'_{\mathrm{Sp}(6)}$ and H'_{PDS} spectra. More specifically, we have plotted the contributions from the SU(3) irreps at $0\hbar\omega$ and $2\hbar\omega$, as well as the (summed) contributions from $4\hbar\omega$ and $6\hbar\omega$ excitations.

As in the previous examples, we observe that the eigenstates of both Hamiltonians have very similar structures: For a given state, the same $N\hbar\omega$ level of excitation is dominant in both calculations and, moreover, within this dominant excitation, we find similar SU(3) distributions. The structural differences that do exist are, again, reflected in the very sensitive interband transition rates, as can be seen in Table VI.

VI. COMPARISON OF PARTIAL SYMMETRIES IN BOSONIC AND FERMIONIC MANY-BODY SYSTEMS

Partial dynamical symmetries were first studied in the interacting boson model (IBM) of nuclei [6]. In [17], the following IBM Hamiltonian was used to reproduce measured energies and $E2$ rates of ^{168}Er:

$$H_{IBM}(h_0,h_2)=h_0P_0^{\dagger}P_0+h_2P_2^{\dagger}\cdot\tilde{P}_2, \qquad (37)$$

TABLE VI. Comparison of intraband and interband $B(E2)$ rates for ^{24}Mg. Shown are selected transitions between states of the $K=0_1$, 0_2, 0_3, and 2_2 bands. The PDS values are rescaled by $e^*=1.75$. Ratios of the results from the two theoretical approaches are given in the last column.

Transition				Model $B(E2)$ (W.u.)		$\frac{B(E2)[\mathrm{PDS}]}{B(E2)[\mathrm{Sp6}]}$
J_i	K_i	J_f	K_f	Sp(6,R)	PDS	
2	0_1	0	0_1	20.4	20.5	1.00
2	0_2	0	0_1	5.6	10.2	1.84
2	0_3	0	0_1	0.047	0.19	4.09
2	2_2	0	0_1	0.22	2.1	9.46
2	0_1	0	0_2	2.5	5.2	2.05
2	0_2	0	0_2	14.8	26.6	1.80
2	0_3	0	0_2	0.037	0.047	1.26
2	2_2	0	0_2	0.48	3.4	7.00
2	0_1	0	0_3	0.025	0.042	1.69
2	0_2	0	0_3	0.12	0.12	1.06
2	0_3	0	0_3	12.9	16.2	1.26
2	2_2	0	0_3	0.023	0.12	5.21
4	0_1	2	0_1	26.9	26.2	0.97
4	0_2	2	0_1	9.7	18.4	1.90
4	0_3	2	0_1	0.052	0.48	9.20
4	2_2	2	0_1	0.66	0.21	0.32

where h_0, h_2 are arbitrary parameters and $P^\dagger_L$, $L=0$ and 2, are boson pair operators:

$$P^\dagger_0 = d^\dagger \cdot d^\dagger - 2(s^\dagger)^2,$$

$$P^\dagger_{2\mu} = 2s^\dagger d^\dagger_\mu + \sqrt{7}(d^\dagger d^\dagger)^{(2)}_\mu. \tag{38}$$

The creation operators $s^\dagger$ and $d^\dagger_\mu$ ($\mu=0,\pm1,\pm2$) denote a monopole boson with angular momentum and parity $J^\pi=0^+$, and a quadrupole boson with $J^\pi=2^+$, respectively. They represent correlated valence nucleon pairs and are the basic building blocks of the IBM. The pair operators $P^\dagger_0$ and $P^\dagger_{2\mu}$ are components of a $(\lambda,\mu)=(0,2)$ SU(3) tensor, and their Hermitian adjoints, P_0 and $\tilde{P}_{2\mu}=(-1)^\mu P_{2,-\mu}$, are characterized by $(\lambda,\mu)=(2,0)$.

It can be shown that for $h_2=h_0$, the Hamiltonian of Eq. (37) becomes a SU(3) scalar [related to the Casimir operator of SU(3)] and for $h_2=-h_0/5$, it transforms as a $(\lambda,\mu)=(2,2)$ SU(3) tensor component. In general, $H_{IBM}(h_0,h_2)$ is, therefore, not a SU(3) scalar, nevertheless it turns out that it always has an exact zero-energy eigenstate, denoted in what follows by $|c;N\rangle$, where the integer N gives the total number of bosons in the system. The state $|c;N\rangle$ describes a condensate of bosons and can be written as

$$|c;N\rangle = \frac{1}{\sqrt{N!}}[(s^\dagger + \sqrt{2}d^\dagger_0)/\sqrt{3}]^N|0\rangle. \tag{39}$$

It is the lowest weight state in the SU(3) irrep $(\lambda,\mu)=(2N,0)$ and serves as an intrinsic state for the SU(3) ground band. The rotational members of the ground band with good angular momentum L are obtained by projection from $|c;N\rangle$. Moreover, one finds that states of the form

$$|k\rangle \propto (P^\dagger_{22})^k|c;N\rangle, \tag{40}$$

are eigenstates of $H_{IBM}(h_0,h_2)$ with eigenvalues $E_k=6h_2(2N+1-2k)k$ and good SU(3) symmetry $(2N-4k,2k)$, where $2k\leqslant N$. They are lowest weight states in these representations and serve as intrinsic states representing γ^k bands with angular momentum projection $K=2k$ along the symmetry axis.

Since $H_{IBM}(h_0,h_2)$ is rotationally invariant, it follows that states of good L projected from $|k=0\rangle=|c;N\rangle$ and $|k\rangle$, $k>0$, are also eigenstates with energy E_k and SU(3) symmetry $(2N-4k,2k)$. The projected states span the entire $(2N,0)$ representation for $k=0$, but only part of the corresponding irrep for $k>0$. There are other excited states that do not preserve the SU(3) symmetry and, therefore, contain a mixture of SU(3) irreps, including the ''special'' irreps $(2N-4k,2k)$. Since $H_{IBM}(h_0,h_2)$ is not a SU(3) scalar, but possesses a subset of solvable eigenstates with good SU(3) symmetry, it is a partial-symmetry Hamiltonian. Adding $\hat{L}^2$, the Casimir operator of SO(3), to $H_{IBM}(h_0,h_2)$ converts the partial symmetry to a partial dynamical symmetry and contributes a $L(L+1)$ splitting, but does not affect the wave functions.

The boson and fermion Hamiltonians, $H_{IBM}(h_0,h_2)$ of Eq. (37) and $H(\beta_0,\beta_2)$ of Eq. (24), have several features in common: Both display partial SU(3) symmetry, they are constructed to be rotationally invariant functions of $(\lambda,\mu)=(2,0)$ and $(\lambda,\mu)=(0,2)$ SU(3) tensor operators, and SU(3) tensor decompositions show that both contain $(\lambda,\mu)=(0,0)$ and (2,2) terms only. $H_{IBM}(h_0,h_2)$, as well as $H(\beta_0,\beta_2)$, has solvable pure-SU(3) eigenstates, which can be organized into rotational bands; the degeneracies within these bands are lifted by adding the SO(3) term $\hat{L}^2$ to the Hamiltonian. The ground bands are pure in both cases, and higher-energy pure bands coexist with mixed-symmetry states.

There are several significant differences between the bosonic and fermionic PDS Hamiltonians, however. For example, the ground band of the Hamiltonian $H_{IBM}(h_0,h_2)$, Eq. (37), is characterized by $(\lambda,\mu)=(2N,0)$, i.e., it describes an axially symmetric prolate nucleus. It is also possible to find an IBM Hamiltonian with partial SU(3) symmetry for an oblate nucleus. It can be shown that these two cases exhaust all possibilities for partial SU(3) symmetry with a two-body Hamiltonian in the IBM-1 with one type of monopole and quadrupole bosons. In contrast, the fermionic Hamiltonians considered here can accommodate ground bands of prolate $[(\lambda_\sigma,0)]$, oblate $[(0,\mu_\sigma)]$, and triaxial $[(\lambda_\sigma,\mu_\sigma)$ with $\lambda_\sigma\neq0$, $\mu_\sigma\neq0]$ shapes.

Another difference between the fermionic and the bosonic PDS cases discussed here lies in the physical interpretation of the excited solvable bands. While these bands represent γ, double γ, etc., excitations in the IBM, they correspond to giant monopole and quadrupole resonances in the fermion case.

Furthermore, whereas the pure eigenstates of $H_{IBM}(h_0,h_2)$ can be generated by repeated action of the boson pair operator $P_{22}^{\dagger}$ on the boson condensate and subsequent angular momentum projection, a similar straightforward construction process for the special eigenstates of $H(\beta_0,\beta_2)$ has not been identified yet. The situation seems to be more complicated in the fermion case, which is also reflected in the fact that $H(\beta_0,\beta_2)$ has two possible families of pure eigenstates, one finite, the other infinite. The association of the special states to one or the other family depends on the $0\hbar\omega$ symplectic starting configuration.

The comparison of partial dynamical symmetries in bosonic and fermionic systems above illustrates that, in spite of similar algebraic structures of the associated Hamiltonians, two given systems with partial symmetries may exhibit not only different physical interpretations, but also different systematic features and different mechanisms for generating the partial symmetries in question.

VII. SUMMARY AND CONCLUSIONS

The fundamental concept underlying algebraic theories in quantum physics is that of an exact or dynamical symmetry. Realistic quantum systems, however, often require the associated symmetry to be broken in order to allow for a proper description of some observed basic features. Partial dynamical symmetry describes an intermediate situation in which some eigenstates exhibit a symmetry that the associated Hamiltonian does not share. The objective of this approach is to remove undesired constraints from the theory while preserving the useful aspects of a dynamical symmetry, such as solvability, for a subset of eigenstates.

We have presented an example of a partial dynamical symmetry in an interacting many-fermion system. In the framework of the symplectic shell model, we have constructed a family of rotationally invariant Hamiltonians with partial SU(3) symmetry. We have demonstrated that the PDS Hamiltonians are closely related to the deformation inducing quadrupole-quadrupole interaction and break SU(3) symmetry, but still possess a subset of ''special'' solvable eigenstates that respect the symmetry. The construction process for these special states was outlined and analytic expressions for their energies and for $E2$ transition rates between them were given.

To illustrate that the PDS Hamiltonians introduced here are physically relevant, we have presented applications to oblate, prolate, and triaxially deformed nuclei. Specifically, we have compared the energy spectra, reduced quadrupole transition strengths, and eigenstate structures of the partial-symmetry Hamiltonians to those of a symplectic shell-model Hamiltonian containing a realistic quadrupole-quadrupole interaction. Although the PDS Hamiltonians cannot account for intershell correlations, we have observed that various features of the quadrupole-quadrupole interaction are reproduced with a particular parametrization of the partial-symmetry Hamiltonians. PDS eigenfunctions do not contain admixtures from different $N\hbar\omega$ configurations, but belong entirely to one level of excitation. We have found that, for reasonable interaction parameters, the $N\hbar\omega$ level to which a particular PDS band belongs is also dominant in the corresponding band of exact $Q_2\cdot Q_2$ eigenstates. Moreover, within this dominant excitation, eigenstates of both Hamiltonians have similar SU(3) distributions. Structural differences, nevertheless, do arise and are reflected in the very sensitive interband transition rates. Overall, however, we may conclude that PDS eigenstates approximately reproduce the structure of the exact $Q_2\cdot Q_2$ eigenstates, for both ground and most resonance bands.

The notion of partial dynamical symmetries extends and complements the familiar concepts of exact and dynamical symmetries. It is applicable when a subset of physical states exhibit a symmetry that does not arise from the invariance properties of the relevant Hamiltonian. Recent studies, including the one presented here, show that partial symmetries may indeed be realized in various quantum systems. This indicates that PDS is not a mere mathematical concept, but may serve as a practical tool in realistic applications of algebraic methods to physical systems.

ACKNOWLEDGMENTS

The authors appreciate valuable discussions with D.J. Rowe, J.P. Elliott, and G. Rosensteel during a visit to the Institute for Nuclear Theory at the University of Washington. This work was supported in part by the Israel Science Foundation.

APPENDIX A: SU(3) WIGNER COEFFICIENTS AND WIGNER-ECKART THEOREM

If α represents a set of labels used to distinguish orthonormal basis states within a given irreducible SU(3) representation (λ,μ), the Wigner coefficients $\langle(\lambda_1,\mu_1)\alpha_1;(\lambda_2,\mu_2)\alpha_2|(\lambda,\mu)\alpha\rangle_\rho$ are defined as the elements of a unitary transformation between coupled and uncoupled orthonormal irreps of SU(3) in the α scheme [40],

$$|(\lambda,\mu)\alpha\rangle_\rho=\sum_{\alpha_1\alpha_2}\langle(\lambda_1,\mu_1)\alpha_1;(\lambda_2,\mu_2)\alpha_2|(\lambda,\mu)\alpha\rangle_\rho|(\lambda_1,\mu_1)\alpha_1\rangle|(\lambda_2,\mu_2)\alpha_2\rangle, \tag{A1}$$

and the inverse transformation is given by

$$|(\lambda_1,\mu_1)\alpha_1\rangle|(\lambda_2,\mu_2)\alpha_2\rangle=\sum_{\rho(\lambda,\mu)\alpha}\langle(\lambda_1,\mu_1)\alpha_1;(\lambda_2,\mu_2)\alpha_2|(\lambda,\mu)\alpha\rangle_\rho|(\lambda,\mu)\alpha\rangle_\rho. \tag{A2}$$

Here $\alpha=\epsilon\Lambda M_\Lambda$ for the SU(3)$\supset$SU(2)$\otimes$U(1) (canonical) group chain and $\alpha=\kappa lm$ for the SU(3)$\supset$SO(3) reduction employed in this work. The subgroup chains impose certain restrictions on the above couplings, for example, the usual angular momentum coupling rules, $l=l_1+l_2,\ \ldots,\ |l_1-l_2|$, and $m=m_1+m_2$ apply for the chain containing SO(3).

The outer multiplicity label $\rho=1,2,\ldots,\rho_{max}$ is used to distinguish multiple occurrences of a given (λ,μ) in the direct product $(\lambda_1,\mu_1)\times(\lambda_2,\mu_2)$: $\rho=1,2,\ldots,\rho_{max}$, where ρ_{max} denotes the number of possible couplings $(\lambda_1,\mu_1)\times(\lambda_2,\mu_2)$, and the possible (λ,μ) irreps in the product can be obtained by coupling the appropriate Young diagrams [3]. O'Reilly [66] determines a closed formula for the decomposition of the outer product $(\lambda_1,\mu_1)\times(\lambda_2,\mu_2)$ of SU(3) irreps for arbitrary positive integers λ_i,μ_i, and derives necessary and sufficient conditions for a SU(3) irrep (λ,μ) to appear as summand in $(\lambda_1,\mu_1)\times(\lambda_2,\mu_2)$.

It is possible to factor out the dependence of the above SU(3)$\supset$SO(3) Wigner coupling coefficient on the m subgroup label by defining so-called double-barred or "reduced" SU(3) coupling coefficients,

$$\begin{aligned}&\langle(\lambda_1,\mu_1)\kappa_1 l_1 m_1;(\lambda_2,\mu_2)\kappa_2 l_2 m_2|(\lambda,\mu)\kappa lm\rangle_\rho\\&\quad=\underbrace{\langle(\lambda_1,\mu_1)\kappa_1 l_1;(\lambda_2,\mu_2)\kappa_2 l_2||(\lambda,\mu)\kappa l\rangle_\rho}_{\text{reduced Wigner coefficient}}\ \underbrace{\langle l_1 m_1, l_2 m_2|lm\rangle}_{\text{geometric part}}.\end{aligned}\tag{A3}$$

The "geometric" part $\langle\cdots|\cdot\rangle$ is simply a SU(2) Clebsch-Gordan coefficient. From the unitarity of the full SU(3) Wigner and the ordinary SU(2) Clebsch-Gordan coefficients it follows that the double-bar coefficients are also unitary. With the phase convention introduced in Ref. [40] they become real, and therefore orthogonal. Draayer and Akiyama [40] give a prescription for the unique determination, including the phases, of SU(3) Wigner coefficients and derive their relevant conjugation and symmetry properties. They furthermore provide a computer code that allows for a numerical determination of the coefficients [51]. Analytic expressions for Wigner coefficients that are of particular interest in p shell and ds shell nuclear shell-model calculations are tabulated in Ref. [67] for the canonical subgroup chain and in Refs. [43,53,68] for the SU(3)$\supset$SO(3) chain.

The Wigner-Eckart theorem for the group SU(2) yields SU(2)-reduced (double-bar) matrix elements of a SO(3) irreducible tensor operator,

$$\langle l_3 m_3|T^{l_2 m_2}|l_1 m_1\rangle=\langle l_1 m_1;l_2 m_2|l_3 m_3\rangle\frac{\langle l_3||T^{l_2}||l_1\rangle}{\sqrt{2l_3+1}}.\tag{A4}$$

Analogously, the generalized Wigner-Eckart theorem allows one to express matrix elements of SU(3) irreducible tensor operators as a sum over ρ of the product of a ρ dependent generalized reduced matrix element multiplied by the corresponding Wigner coefficient [40],

$$\begin{aligned}&\langle(\lambda_3,\mu_3)\alpha_3|T^{(\lambda_2,\mu_2)\alpha_2}|(\lambda_1,\mu_1)\alpha_1\rangle\\&\quad=\sum_\rho\langle(\lambda_1,\mu_1)\alpha_1;(\lambda_2,\mu_2)\alpha_2|(\lambda_3,\mu_3)\alpha_3\rangle_\rho\\&\qquad\times\langle(\lambda_3,\mu_3)|||T^{(\lambda_2,\mu_2)}|||(\lambda_1,\mu_1)\rangle_\rho.\end{aligned}\tag{A5}$$

For more details on SU(3) coupling and recoupling coefficients, see the compilation in Appendix C of Ref. [36] and references therein.

APPENDIX B: MATRIX ELEMENTS OF RELEVANT OPERATORS

The calculations presented here require expressions for matrix elements of the Sp(6,R) generators $\hat{A}^{(20)}$, $\hat{B}^{(02)}$, and $\hat{C}^{(11)}$, and combinations thereof. None of these operators connect states belonging to different symplectic representations and, furthermore, the SU(3) generators $\hat{C}^{(11)}_{1q}=\hat{L}_q$ and $\hat{C}^{(11)}_{2\mu}=1/\sqrt{3}Q^E_{2\mu}$ act only within one level of excitation N. Matrix elements for $\hat{C}^{(11)}$ in the standard SU(3) bases are given by [49,67],

$$\begin{aligned}&\langle(\lambda',\mu')|||\hat{C}^{(11)}|||(\lambda,\mu)\rangle\\&\quad=(-1)^{\phi_\mu}\sqrt{2\langle\hat{C}_{\mathrm{SU}(3)}\rangle[(\lambda,\mu)]}\,\delta_{(\lambda',\mu')(\lambda,\mu)},\end{aligned}\tag{B1}$$

where $\hat{C}_{\mathrm{SU}(3)}$ denotes the second-order Casimir operator of SU(3), given in Eq. (9), and $\phi_\mu=1$ for $\mu\neq0$ and $\phi_\mu=0$ for $\mu=0$. The reduced matrix element $\langle(\lambda',\mu')|||\hat{C}^{(11)}|||(\lambda,\mu)\rangle$ is related to the full SU(3) matrix element via the Wigner-Eckart theorem for SU(3) and the phase is chosen to be consistent with that of Ref. [49].

Several strategies for calculating matrix elements of the symplectic generators $\hat{A}^{(20)}$ and $\hat{B}^{(02)}$ have been explored. A direct way is to use the Sp(6,R) commutation relations to derive recursion formulas, as shown by Rosensteel [35]. Another approach is to start from approximate matrix elements and to proceed by successive approximations, adjusting the matrix elements until the commutation relations are precisely satisfied [29]. Deenen and Quesne [69] have employed a

boson mapping to obtain generator matrix elements, and Castaños *et al.* [70] have derived simple analytical functions for some special irreps. The most elegant method, outlined by Rowe in Ref. [71], involves vector-valued coherent state representation theory and evaluates matrix elements of the symplectic raising and lowering operators by relating them to the matrix elements of a much simpler u(3)⊗Weyl algebra. A listing of the relevant formulas is beyond the scope of this appendix, the reader is thus referred to Ref. [71] for details of the calculation.

Matrix elements of the SU(3)⊃SO(3) integrity basis operators $\hat{X}_3 \equiv (\hat{L}\times Q^E)_{(1)}\cdot\hat{L}$ and $\hat{X}_4 \equiv (\hat{L}\times Q^E)_{(1)}\cdot(\hat{L}\times Q^E)_{(1)}$ can be given in terms of SO(3) Racah recoupling coefficients $W(l_1,l_2,l,l_3;l_{12},l_{23})$ [72] and the SU(3)⊃SO(3) reduced matrix elements of $\hat{C}^{(11)}$ [49],

$$\langle(\lambda,\mu)\kappa l m|\hat{X}_3|(\lambda',\mu')\kappa' l' m'\rangle = \delta_{(\lambda',\mu')(\lambda,\mu)}\delta_{l'l}\delta_{m'm}3l(l+1)\sqrt{2l+1}W(l,1,l,1;l,2) \times\langle(\lambda,\mu)\kappa l||\hat{C}_2^{(11)}||(\lambda,\mu)\kappa' l\rangle; \quad \text{(B2)}$$

$$\langle(\lambda,\mu)\kappa l m|\hat{X}_4|(\lambda',\mu')\kappa' l' m'\rangle = \delta_{(\lambda',\mu')(\lambda,\mu)}\delta_{l'l}\delta_{m'm}9l(l+1) \times\sqrt{2l+1}\sum_{\kappa'' l''}(-1)^{l+l''+1}\sqrt{2l''+1}[W(1,l,2,l'';l,1)]^2 \times\langle(\lambda,\mu)\kappa l||\hat{C}_2^{(11)}||(\lambda,\mu)\kappa'' l''\rangle \times\langle(\lambda,\mu)\kappa'' l''||\hat{C}_2^{(11)}||(\lambda,\mu)\kappa' l\rangle. \quad \text{(B3)}$$

[1] J.P. Elliott and P.G. Dawber, *Symmetry in Physics* (Oxford University Press, New York, 1979), Vols. 1 and 2.

[2] *Dynamical Groups and Spectrum Generating Algebras*, edited by A. Bohm, Y. Ne'eman, and A. O. Barut (World Scientific, Singapore, 1988).

[3] M. Hamermesh, *Group Theory and its Applications to Physical Problems* (Dover, New York, 1989).

[4] J. Fuchs and C. Schweigert, *Symmetries, Lie Algebras and Representations* (Cambridge University Press, Cambridge, 1997).

[5] M. Gell-Mann and Y. Ne'eman, *The Eightfold Way* (Benjamin, New York, 1964); H. Georgi, *Lie Algebras in Particle Physics* (Benjamin, Reading, MA, 1982).

[6] F. Iachello and A. Arima, *The Interacting Boson Model* (Cambridge University Press, Cambridge, 1987); D. Bonatsos, *Interacting Boson Models of Nuclear Structure* (Oxford University Press, Oxford, 1988); F. Iachello and P. Van Isacker, *The Interacting Boson-Fermion Model* (Cambridge University Press, Cambridge, 1991).

[7] *Group Theory and Special Symmetries in Nuclear Physics*, edited by J.P. Draayer and J. Jänecke (World Scientific, Singapore, 1992).

[8] *Algebraic Approaches to Nuclear Structure*, edited by R.F. Casten (Harwood Academic, Chur, 1993).

[9] I. Talmi, *Simple Models of Complex Nuclei* (Harwood Academic, Chur, 1993).

[10] D.J. Rowe, Prog. Part. Nucl. Phys. **37**, 265 (1996).

[11] *Latin-American School of Physics XXX ELAF*, edited by O. Castaños, R. López-Pena, J. G. Hirsch, and K. B. Wolf, AIP Conf. Proc. No. 365 (AIP, Woodbury, NY, 1996).

[12] F. Iachello and R.D. Levine, *Algebraic Theory of Molecules* (Oxford University Press, Oxford, 1994).

[13] Y. Alhassid and A. Leviatan, J. Phys. A **25**, L1265 (1992); A. Leviatan, *Symmetry in Science VII* (Plenum Press, New York, 1994), p. 383.

[14] A.G. Ushveridze, *Quasi-Exactly Solvable Models in Quantum Mechanics* (Institute of Physics, Bristol, 1994).

[15] P. Van Isacker, Phys. Rev. Lett. **83**, 4269 (1999).

[16] C. Bahri, D.J. Rowe, and W. Wijesundera, Phys. Rev. C **58**, 1539 (1998); C. Bahri and D.J. Rowe, Nucl. Phys. **A662**, 125 (2000).

[17] A. Leviatan, Phys. Rev. Lett. **77**, 818 (1996).

[18] I. Sinai, M.Sc. thesis, The Hebrew University, 1998.

[19] A. Leviatan and I. Sinai, Phys. Rev. C **60**, 061301 (1999); J. Phys. G **25**, 791 (1999).

[20] I. Talmi, Phys. Lett. B **405**, 1 (1997).

[21] A. Arima, T. Otsuka, F. Iachello, and I. Talmi, Phys. Lett. **66B**, 205 (1977): T. Otsuka, A. Arima, F. Iachello, and I. Talmi, *ibid.* **76B**, 139 (1978).

[22] A. Leviatan and J. N. Ginocchio, Phys. Rev. C **61**, 024305 (2000).

[23] R.V. Jolos and P. von Brentano, Phys. Rev. C **62**, 034310 (2000).

[24] R.V. Jolos and P. von Brentano, Phys. Rev. C **63**, 024304 (2001).

[25] J.L. Ping and J.Q. Chen, Ann. Phys. (N.Y.) **255**, 75 (1997).

[26] N.D. Whelan, Y. Alhassid, and A. Leviatan, Phys. Rev. Lett. **71**, 2208 (1993); A. Leviatan and N.D. Whelan, *ibid.* **77**, 5202 (1996).

[27] E. Canetta and G. Maino, Phys. Lett. B **483**, 55 (2000).

[28] J. Escher and A. Leviatan, Phys. Rev. Lett. **84**, 1866 (2000).

[29] G. Rosensteel and D.J. Rowe, Phys. Rev. Lett. **38**, 10 (1977); Ann. Phys. (N.Y.) **126**, 343 (1980); D.J. Rowe, Rep. Prog. Phys. **48**, 1419 (1985).

[30] M. Mamistvalov, M.Sc. thesis, The Hebrew University, 1999.

[31] D.J. Rowe and G. Rosensteel, Phys. Rev. Lett. **87**, 172501 (2001).

[32] F. Arickx, Nucl. Phys. **A268**, 347 (1976).

[33] F. Arickx, J. Broeckhove, and E. Deumens, Nucl. Phys. **A377**, 121 (1982).

[34] D.R. Peterson and K.T. Hecht, Nucl. Phys. **A344**, 361 (1980).

[35] G. Rosensteel, J. Math. Phys. **21**, 924 (1980).

[36] J. Escher and J.P. Draayer, J. Math. Phys. **39**, 5123 (1998).

[37] G. Rosensteel, in *Group Theory and Special Symmetries in Nuclear Physics* (Ref. [7]), p. 332.

[38] J.P. Elliott, Proc. R. Soc. London, Ser. A **245**, 128 (1958); **245**, 562 (1958).

[39] Here ε, the eigenvalue of Q^E_{20}, gives the U(1) content and the SU(2) irrep is characterized by Λ with projection M_Λ.

[40] J.P. Draayer and Y. Akiyama, J. Math. Phys. **14**, 1904 (1973).
[41] R. Lopez, P.O. Hess, P. Rochford, and J.P. Draayer, J. Phys. A **23**, L229 (1990).
[42] J.P. Draayer, D.L. Pursey, and S.A. Williams, Nucl. Phys. **A119**, 577 (1968): J.P. Draayer and S.A. Williams, *ibid.* **A129**, 647 (1969).
[43] J.D. Vergados, Nucl. Phys. **A111**, 681 (1968).
[44] Vergados projects from a state with $\varepsilon=\varepsilon_{min}=-\lambda-2\mu$, $\Lambda=\lambda/2$, $M_\Lambda=\lambda/2$ for $\lambda\geqslant\mu$ and $\varepsilon=\varepsilon_{max}=2\lambda+\mu$, $\Lambda=\mu/2$, $M_\Lambda=-\mu/2$ for $\lambda<\mu$ and employs the ''Elliott rule'' to determine the possible K values, $K=\min(\lambda,\mu), \min(\lambda,\mu)-2, \ldots,$ 1 or 0, and angular momenta, $L=K$, $K+1$, $K+2, \ldots, K+\max(\lambda,\mu)$ for $K\neq 0$ and $L=\max(\lambda,\mu), \max(\lambda,\mu)-2, \ldots,$ 1 or 0 for $K=0$. It is also possible to project from $\varepsilon=\varepsilon_{max}$, $\Lambda=\mu/2$, and $M_\Lambda=+\mu/2$ or $\varepsilon=\varepsilon_{min}$, $\Lambda=\lambda/2$, $M_\Lambda=-\lambda/2$. Draayer *et al.* [40,42] discuss the different projection possibilities and give rules analogous to the Elliott rule for determining the K and L content of a given SU(3) irrep (λ,μ).
[45] J.P. Draayer, in *Algebraic Approaches to Nuclear Structure* (Ref. [8]), p. 423.
[46] G. Rosensteel and J.P. Draayer, and K.J. Weeks, Nucl. Phys. **A419**, 1 (1984).
[47] O. Castaños and J.P. Draayer, Nucl. Phys. **A491**, 349 (1989).
[48] Higher-order rotational scalars in Q_2 can be included in V_{coll} in order to accommodate more complicated potential forms, e.g., a cubic term introduces a γ dependence into the potential.
[49] J.P. Draayer and G. Rosensteel, Nucl. Phys. **A439**, 61 (1985).
[50] G. Rosensteel, Phys. Rev. C **42**, 2463 (1990).
[51] Y. Akiyama and J.P. Draayer, Comput. Phys. Commun. **5**, 405 (1973).
[52] K.T. Hecht, J. Phys. A **23**, 407 (1990).
[53] S.S. Avancini and E.J.V. de Passos, J. Phys. G **19**, 125 (1993).
[54] W.J. Vermeer, M.T. Esat, J.A. Kuehner, R.H. Spear, A.M. Baxter, and S. Hinds, Phys. Lett. **122B**, 23 (1983).
[55] F. Ajzenberg-Selove, Nucl. Phys. **A506**, 1 (1990).
[56] J.P. Draayer, K.J. Weeks, and G. Rosensteel, Nucl. Phys. **A413**, 215 (1984).
[57] Y. Suzuki, Nucl. Phys. **A470**, 119 (1987).
[58] D.R. Tilley, C.M. Cheves, J.H. Kelley, S. Raman, and H.R. Weller, Nucl. Phys. **A636**, 249 (1998).
[59] P. Raghavan, At. Data Nucl. Data Tables **42**, 189 (1989).
[60] R.H. Spear, Phys. Rep. **73**, 369 (1981).
[61] E.J. Reske, Ph.D. thesis, University of Michigan, 1984.
[62] J. Escher and J.P. Draayer, Phys. Rev. Lett. **82**, 5221 (1999).
[63] D. Branford, A.C. McGough, and I.F. Wright, Nucl. Phys. **A241**, 349 (1975).
[64] P.M. Endt, At. Data Nucl. Data Tables **55**, 171 (1993).
[65] Note that we have used the experimental $B(E2)$ values from Ref. [63], which contains a more complete list of $B(E2)$ data than the compilation by Endt [64]. The latter gives values of 20.6 ± 0.4 W.u., 35 ± 5 W.u., and 37 ± 12 W.u. for the first three transitions listed in Table V. Fitting the symplectic Hamiltonian parameters to reproduce the values of Ref. [64] gives results very similar to the ones presented here and does not alter our conclusions.
[66] M.F. O'Reilly, J. Math. Phys. **23**, 2022 (1982).
[67] K.T. Hecht, Nucl. Phys. **A62**, 1 (1965).
[68] K.T. Hecht and Y. Suzuki, J. Math. Phys. **24**, 785 (1982).
[69] J. Deenen and C. Quesne, J. Phys. A **17**, L405 (1984).
[70] O. Castaños, E. Chacón, and M. Moshinsky, J. Math. Phys. **25**, 1211 (1984).
[71] D.J. Rowe, J. Math. Phys. **25**, 2662 (1984).
[72] D.A. Varshalovich, A.N. Moskalev, and V.K. Kersonskii, *Quantum Theory of Angular Momentum* (World Scientific, Singapore, 1988).